THE ASTROPHYSICAL JOURNAL, 544:780–804, 2000 December 1

AN X-RAY, OPTICAL, AND RADIO SEARCH FOR SUPERNOVA REMNANTS IN THE NEARBY SCULPTOR GROUP Sd GALAXY NGC 300

THOMAS G. PANNUTI
MIT Center for Space Research, NE80-6015, 70 Vassar Street, Cambridge, MA 02139
NEBOJSA DURIC
Institute for Astrophysics, Department of Physics and Astronomy, University of New Mexico, 800 Yale Boulevard, N.E., Albuquerque, NM 87131
CHRISTINA K. LACEY
Department of Physics and Astronomy, University of South Carolina, Columbia, SC 29208-5320
W. M. GOSS
National Radio Astronomy Observatory, P.O. Box O, Socorro, NM 87801
CHARLES G. HOOPES
Department of Physics and Astronomy, Johns Hopkins University, 3400 N. Charles Street, Baltimore, MD 21218
RENÉ A. M. WALTERBOS
Astronomy Department, New Mexico State University, Box 30001/Dept. 4500, Las Cruces, NM 88003
AND
MARCUS A. MAGNOR
Telecommunications Laboratory, University of Erlangen-Nuremberg, Cauerstrasse 7, 91058 Erlangen, Germany
Received 2000 March 6; accepted 2000 June 23

ABSTRACT

We have conducted a multiwavelength (X-ray, optical, and radio) search for supernova remnants (SNRs) in the nearby Sculptor Group Sd galaxy NGC 300. Our Very Large Array (VLA) radio observations at 6 cm and 20 cm have been combined with previously published optical results, our own optical image, and archived *ROSAT* X-ray data to search for new SNR candidates. Of the 28 optically identified SNRs found by Blair & Long, three exhibit some combination of X-ray and radio emission, but in general X-ray and radio emission from the optically identified SNRs is undetected.

A radio-selected sample of SNR candidates is constructed by searching for positional coincidences between nonthermal radio continuum sources and sources of Hα emission with the intent of finding SNRs that are typically overlooked using the [S II]/Hα criterion, i.e., those SNRs that are either confused by Hα emission or which are Balmer-dominated. This search has yielded 17 SNR candidates, of which 14 are new and three were already known from the optically selected sample. Four of the radio-selected candidates also possess detectable X-ray emission.

A complementary analysis of the X-ray data has yielded an X-ray–selected sample of candidates consisting of six soft-spectrum sources ($kT < 1$ keV) coincident with regions of Hα emission. Two of these candidate X-ray SNRs are common to the radio-selected sample and two more are common to the optically selected sample. Thus, the X-ray selection has yielded two additional candidates.

Through a multiwavelength campaign, we have added sixteen new candidate SNRs to the 28 previously known SNRs for a total of 44 SNR candidates in NGC 300. The fact that these new candidates were missed in the optical surveys suggests a possible selection effect. SNRs identified through optical methods may represent only the SNRs located in regions with relatively low confusion from Hα emission, well away from star-forming regions. The SNRs in or near star-forming regions are more likely to be confused by emission from H II regions and are therefore more likely to be missed in optical surveys. The radio-selection process, on the other hand, suffers from a separate selection effect: it can only identify candidates if they are associated with H II regions, such that our sample of radio-selected SNRs is biased toward star-forming regions. Finally, the X-ray candidates are selected on the basis of having soft spectra and association with H II regions, so that the sample is biased against X-ray–emitting SNRs with hard spectra and no optical counterparts. The fact that the optically selected, radio-selected, and X-ray–selected data sets of SNR candidates have limited overlap is consistent with these opposing selection effects. We present a simulation to investigate the effects of optical confusion on a hypothetical optical survey for SNRs in a galaxy, using "artificial" SNRs that have been placed in a range of confused environments. We find that the detection of SNRs becomes increasingly difficult with distance, and that the most deeply embedded SNRs are not identified even in the nearest distance investigated. We conclude that a multifrequency search for SNRs is required to uniformly sample the SNR population of a galaxy.

Subject headings: galaxies: individual (NGC 300) — galaxies: ISM — galaxies: spiral — radio continuum: galaxies — supernova remnants — X-rays: galaxies

1. INTRODUCTION

Traditionally, searches for supernova remnants (SNRs) have concentrated on detections of sources that are located within the Galaxy. Unfortunately, these Galactic searches are fraught with difficulties arising from absorption and extinction within the plane of the Milky Way and the Sun's location within the Galactic disk. In contrast, nearby galaxies can be considered better choices for SNR searches, especially those galaxies with nearly face-on orientations and high Galactic latitude locations that minimize both Galactic absorption and absorption internal to the host galaxies.

A multiwavelength approach is necessary to identify a source as a SNR, since an observation through a single spectral window cannot identify all types of SNRs. The three wavelength regimes that have been used most commonly for SNR surveys have been the X-ray, optical, and radio domains (see Magnier et al. 1995 for a review). A SNR can be a prominent source in each of these bands for different reasons. The expanding SNR shock heats the surrounding interstellar medium (ISM) to temperatures of 10^6–10^7 K, producing X-ray emission (e.g., Itoh & Masai 1989), while electrons gyrating in the SNR's magnetic field produce synchrotron radiation at radio frequencies (e.g., Duric et al. 1995). A SNR can also be detected optically by emission from collisionally ionized species such as [S II], [N II] and [O III], as well as Hα recombination emission. The degree to which a SNR becomes an X-ray, radio or optical emission line source and the relative strengths of each of these radiative signatures are most likely a function of environment and the evolutionary stage of the SNR. The details, however, are poorly understood, and these considerations have motivated our multifrequency survey of SNRs.

Pioneering work in this field was conducted by Mathewson & Clarke (1972, 1973a, 1973b), who searched for SNRs in the Magellanic Clouds by combining optical observations of emission from the atomic species mentioned above with radio observations. Candidate optical sources were identified by examining image-tube plates taken through filters that isolated the emission lines of Hα + [N II] and [S II], and simultaneous radio surveys of these galaxies at the frequency of 408 MHz sought to identify nonthermal sources (therefore candidate SNRs). These studies yielded 12 SNRs in the Large Magellanic Cloud and two in the Small Magellanic Cloud. Subsequent optical surveys for SNRs probed the major Local Group spirals M31 (Blair, Kirschner, & Chevalier 1981; Braun & Walterbos 1993; Magnier et al. 1995) and M33 (Long et al. 1990; Smith et al. 1993; Gordon et al. 1998, 1999). D'Odorico, Dopita, & Benvenuti (1980, hereafter DDB80) independently searched for SNRs in these two galaxies, as well as two other Local Group galaxies (the irregulars NGC 6822 and IC 1613). In addition, galaxies outside of the Local Group (NGC 253, NGC 300, IC 342, and NGC 2403) were also investigated.

Advances in technology and instrumentation have increased the sensitivity and resolution that may be used for these kinds of surveys. Thus, galaxies can now be examined in more detail, allowing the confirmation or refutation of previously identified SNRs as well as the detections of new ones. An example of recent work in this field for galaxies located outside of the Local Group include Blair & Long (1997) (hereafter BL97), who performed an optical survey for SNRs by comparing [S II] and Hα images of the Sculptor Group galaxies NGC 300 and NGC 7793 and found a total of 56 SNRs in these two galaxies. Sources that featured a [S II]/Hα ratio of 0.4 or higher were classified as SNRs by those authors. In addition, two other optical surveys for extragalactic SNRs conducted by Matonick & Fesen (1997) and Matonick et al. (1997) also compared [S II] and Hα images of six target galaxies, using a somewhat more stringent identification criterion (namely, only sources with a [S II]/Hα ratio of 0.45 or higher were identified as SNRs). Those two surveys found 35 SNRs in NGC 2403 (Matonick et al. 1997), three SNRs in NGC 5204, five in NGC 5585, 27 in NGC 6946, 41 in M81, and 93 in M101 (Matonick & Fesen 1997).

X-ray and radio observations can complement these optical surveys by providing additional spectral information about the optically identified SNRs and by locating SNRs that have escaped detection by optical surveys. Such observations can provide evidence that a particular source is indeed a SNR if it is detected at another wavelength and can more tightly constrain theoretical models of the spectral evolution of a SNR. Recently, a three-wavelength study like the one presented in this paper was applied by Lozinskaya et al. (1998) to the study of the SNR S8 in IC 1613. X-ray, optical, and radio studies of this SNR were able to demonstrate the youth of this SNR (3–6×10^3 years) as well as to probe the density of the interstellar medium surrounding the SNR ($n_e \sim 1$ cm^{-3}). Intensive campaigns like the one presented in this paper are intended to contribute significantly to our knowledge of the environments and evolution of SNRs, and how the two are related.

In the present paper we report the results of a multiwavelength search campaign for SNRs in the nearby Sculptor Group Sd spiral galaxy NGC 300, based on our examination of *ROSAT* X-ray observations of this galaxy, our own radio observations at 6 and 20 cm, the optical data presented in BL97, and our own Hα image of the galaxy. NGC 300 lies at a distance of 2.1 Mpc (Freedman et al. 1992) and is a member of the Sculptor Group of galaxies (Puche & Carignan 1988). We list several relevant properties of this galaxy in Table 1. Because of the high Galactic latitude (and corresponding low foreground neutral hydrogen column density), low inclination angle, relative proximity, and large spatial extent, NGC 300 has often been chosen as a test of global spiral galaxy properties. Examples of such works include a study of the galaxy's H II regions

TABLE 1

GENERAL PROPERTIES OF NGC 300

Property	Value
R.A. (J2000.0)	$00^h54^m53\overset{s}{.}47$[a]
Decl. (J2000.0)	$-37°41'00''$[a]
Galactic latitude	−79.42
Galactic longitude	299.22[b]
Observed diameter D_{25} (arcmin)	20.2[b]
Axial ratio d/D	0.75[b]
N_H Column Density (cm^{-2})	2.97×10^{20}[c]
Hubble type	SA(s)d[a]
Distance (Mpc)	2.1[d]
Inclination i (deg)	46[b]

[a] NED Database.
[b] Tully 1988.
[c] RPS97.
[d] Freedman et al. 1992.

and metallicity gradient (Deharveng et al. 1988, hereafter D88), a study of the kinematics of the galaxy's H I distribution (Puche, Carignan, & Bosma 1990), a study of the galaxy's Cepheid variables based on *BVRI* photometry (Freedman et al. 1992), and a study of the galaxy's diffuse ionized gas (DIG) (Hoopes, Walterbos, & Greenawalt 1996, hereafter HWG96).

The goal of the present study is to make use of the multiple wavelength data to obtain new detections of SNRs in this galaxy and to use this method of multiwavelength comparisons as a template for future surveys of additional galaxies. The observations and data analysis are discussed in § 2, beginning with the radio observations in § 2.1, followed by the optical observations in § 2.2, and concluding with the X-ray observations in § 2.3. The optically identified SNRs found by BL97 were examined for X-ray and radio emission, and the results of these investigations are presented in § 3. To complement the previous optical surveys for SNRs in this galaxy, we searched for new candidate SNRs based on radio and X-ray–selected sources. In § 4, we present the results of our search for new radio-selected candidates, and the results of our search for new X-ray–selected candidates are presented in § 5. A discussion of the spectral properties of the detected candidate SNRs and the usefulness of a multiwavelength approach for surveys of extragalactic SNRs is presented in § 6. To investigate the effects of confusion and distance inherent in optical searches for SNRs in nearby galaxies, we present a simulation using "artificial" SNRs added to our Hα image and analyze the results in § 6.2. Finally, our conclusions are given in § 7.

2. OBSERVATIONS AND DATA REDUCTION

2.1. *Radio Observations and Data Reduction*

We observed NGC 300 with the Very Large Array (VLA) of the National Radio Astronomy Observatory (NRAO[1]) at a wavelength of 6 cm in the hybrid CnB configuration (northern arm in the B array) on 1993 May 22, and at a wavelength of 20 cm in the BnA configuration on 1998 June 13. These hybrid arrays are better suited for studying sources situated at southern declinations (such as NGC 300) because of the greater north-south coverage provided by the extended northern arm. The approximate beam sizes in the final images are $\approx 4''$ at 6 cm (4885 MHz) and $\approx 6''$ at 20 cm (1465 MHz). The RMS noise, measured in each image, is 36 μJy beam^{-1} at 6 cm and 60 μJy beam^{-1} at 20 cm. Details of the VLA observations are listed in Table 2.

In order to minimize bandwidth smearing, which limits the field of view when observing in normal continuum mode, we observed NGC 300 in multichannel line mode with seven channels per IF and a channel width of 3.125 MHz, thereby synthesizing a total band of 37.5 MHz after dropping the first of the seven channels. The effective observing frequencies for the images made from the remaining six channels were 1.448 GHz (20 cm) and 4.860 GHz (6 cm). Data reduction and analysis were performed using the AIPS software package, which is a standard data reduction package provided by the NRAO. The final images were corrected for primary beam attenuation before undertaking the flux measurements.

The primary goal of the data analysis was to find and measure all discrete sources above a minimum 3 σ detection level. After candidate sources were located, the peak positions were determined by fitting single Gaussians to their emission profiles at 20 cm. The flux density associated with each source was determined using photometric routines in AIPS. We analyzed each source, using annuli approximately $1''$ in width, and determined the flux density based on the cumulative flux density minus the average flux density at an outer annulus chosen to represent the background level.

The spectral index α of each source was calculated from the measured 6 cm and 20 cm flux densities S_6 and S_{20}, respectively. The spectral index α was defined using the convention $S_\nu \propto \nu^{-\alpha}$. The uncertainties in the spectral indices were determined by the propagation of errors. Those radio sources deemed to be nonthermal, on the basis of their spectral indices, formed the set of radio sources from which the radio-selected sample of SNR candidates was constructed (as described in § 4). Properties of these sources (positions in J2000.0 coordinates, flux densities at 6 and 20 cm and spectral indices α) are listed in Table 3.

2.2. *Optical Observations and Data Reduction*

NGC 300 was observed with the 0.6 meter Curtis/Schmidt telescope at the Cerro Tololo Inter-American Observatory (CTIO[2]). Details of the observations and the data reduction can be found in HWG96. Consistent with its Hubble type of Sd, NGC 300 shows extensive star formation throughout its disk, as revealed by the Hα image that reveals a large number of discrete H II regions. In this paper, we will make extensive use of the catalog of H II regions in this galaxy given in D88. In their optical search for candidate SNRs in NGC 300, BL97 identified and analyzed 28 SNRs by comparing the ratio of fluxes of [S II] and Hα emission from sources in this galaxy. The positional accuracy of that sample of optically identified SNRs is $\sim 2''$ (BL97).

Based on the analysis of the DIG within NGC 300, HWG96 found that NGC 300 has a higher fractional DIG luminosity than two other Sculptor galaxies, NGC 55 and NGC 253. A filamentary structure of the DIG in this galaxy was detected, as well as the presence of loop and shell struc-

[1] The National Radio Astronomy Observatory is a facility of the National Science Foundation operated under a cooperative agreement by Associated Universities, Inc.

[2] The CTIO is operated by AURA, Inc., under cooperative agreement with the National Science Foundation as part of the National Optical Astronomy Observatories.

TABLE 2

PARAMETERS OF THE NGC 300 OBSERVATIONS WITH THE VLA

Configuration	Frequency (GHz)	Field of View (arcmin)	RMS Sensitivity (μJy)	Linear Resolution (pc)	Synthesized Beam (arcsec^2)	Position Angle (deg)
CnB.....	4.86	9	36	61	8.6 × 4.2	−3.6
BnA	1.45	27	60	41	4.7 × 3.6	−46.1

TABLE 3

RADIO SOURCES IN NGC 300 – FLUX DENSITIES AND SPECTRAL INDICES

Source Number	R.A. (J2000.0)	Decl. (J2000.0)	S_6 (mJy)	δS_6 (mJy)	S_{20} (mJy)	δS_{20} (mJy)	α[a]	$\delta\alpha$	H II Region
R1.....	00 54 38.2	−37 41 47	<	0.10	0.36	0.07	>1.1	...	D39
R2.....	00 54 38.4	−37 42 42	<	0.10	0.60	0.14	>1.5	...	D40
R3.....	00 54 43.4	−37 43 11	0.27[b]	0.04	0.57[b]	0.10	+0.6	0.2	D53A
R4.....	00 54 44.9	−37 41 10	<	0.10	0.24	0.07	>0.7	...	D60
R5.....	00 54 45.1	−37 41 49	<	0.10	0.23	0.07	>0.7	...	Uncataloged H II region
R6.....	00 54 50.3	−37 40 31	0.14[b]	0.04	0.30	0.10	+0.6	0.4	D76A
R7.....	00 54 51.1	−37 40 59	<	0.10	0.22	0.07	>0.7	...	D80
R8.....	00 54 51.1	−37 41 45	<	0.10	0.30	0.10	>0.9	...	D81
R9.....	00 54 51.3	−37 46 22	<	0.10	0.24	0.07	>0.7	...	D82
R10	00 54 51.8	−37 39 39	0.28[b]	0.07	0.48[b]	0.09	+0.4	0.3	D84
R11	00 55 03.6	−37 42 49	0.28[b]	0.04	0.35[b]	0.11	+0.2	0.3	D118A
R12	00 55 03.7	−37 43 21	0.13[b]	0.04	0.42[b]	0.10	+1.0	0.6	D119A
R13	00 55 12.6	−37 41 38	0.30[b]	0.06	0.50[b]	0.14	+0.4	0.3	D137A
R14	00 55 30.1	−37 39 20	<	0.10	0.28	0.07	>0.9	...	D153

NOTE.—Units of right ascension are hours, minutes, and seconds, and units of declination are degrees, arcminutes, and arcseconds.

[a] $S_\nu \propto \nu^{-\alpha}$

[b] Diffuse radio emission from the adjacent H II region makes isolating the radio emission associated with the SNR difficult at this wavelength.

tures. These features are attributed to supernovae and stellar winds in OB associations. This result indicates that NGC 300 should have a rich SNR population, and therefore this galaxy is an excellent candidate for our study of its resident SNRs at multiple wavelengths. Ferguson et al. (1996) examined the DIG in two other Sculptor Group galaxies, NGC 247 and NGC 7793, and found that between 30% and 50% of the total Hα emission in each galaxy originated from the DIG. In addition, those authors found that widespread massive star formation in both galaxies was the likely origin of the DIG, suggesting that these galaxies will also possess numerous SNRs that may be the subject of a study similar to the one presented in the current paper. An optical survey for SNRs in NGC 7793 has already been performed by BL97, and this galaxy will be the subject of a multiwavelength survey for SNRs that will be presented in a future paper (Pannuti et al. 2000, in preparation). The Hα image of NGC 300 will be used extensively in our analysis of the galaxy's SNRs, as described in §§ 3, 4 and 5.

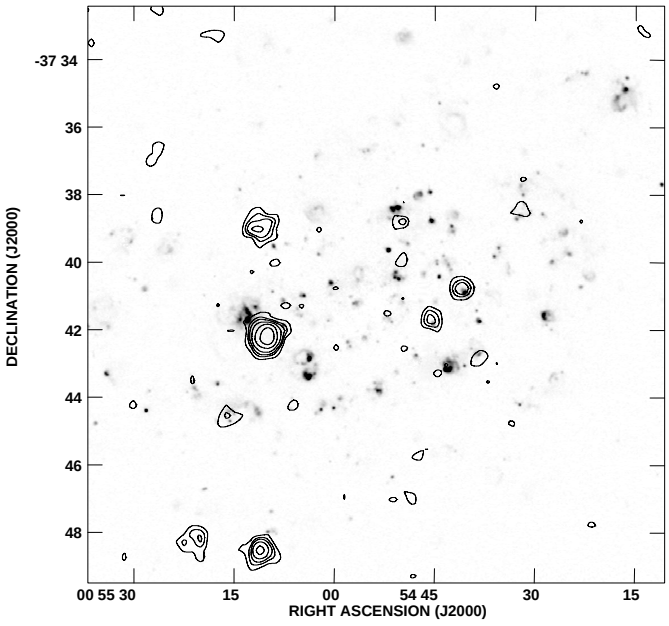

FIG. 1. X-ray (*contours*) and Hα (*gray-scale*) image of NGC 300, taken by the *ROSAT* PSPC instrument, over the total energy range of 0.1–2.4, keV, with a combined integration of 46,306 s. The noise level in the X-ray image is 9.4×10^{-4} counts per square arcminute, and the contours are set at the 3, 6, 9, 15, and 60 σ level.

2.3. *X-Ray Observations and Data Reduction*

We used archived observations of NGC 300 made with the wide-angle, spectral-resolving PSPC (Position Sensitive Proportional Counter) instrument aboard the *ROSAT* satellite. This instrument is capable of imaging X-rays in the energy range of 0.1–2.4 keV with a resolution of $E/\Delta E \sim 2.4E^{-0.5}$, where E is the photon energy in keV (Long et al. 1996). Traditionally, experimenters have divided the PSPC's broad energy range into three channels, corresponding to the "total" band (0.1–2.4 keV), the "hard" (1.0–2.4 keV) band, and the "soft" (0.1–1.0 keV) band (see, for example, the analysis of PSPC observations of M33 given by Long et al. 1996). A more detailed description of the *ROSAT* satellite and its instruments is given by Trümper (1992). NGC 300 was observed for a total of 46 ks over two separate pointings of 37 ks and 9.3 ks, and we obtained images corresponding to these pointings from the Goddard Space Flight Center Image archives. Images at each band from both pointings were combined to prepare individual images at all three bands corresponding to the total integration time of 46 ks.

These PSPC observations of NGC 300 were briefly discussed by Zang, Warwick, & Meurs (1997). Those authors found 19 X-ray sources within a 9′ radius from the center of the galaxy. A detailed survey of the X-ray sources in NGC 300 using the same observation was conducted and presented by Read, Ponman, & Strickland (1997) (hereafter RPS97). RPS97 found 15 sources at the 3σ level or higher associated with NGC 300, and spectral fits of the sources were made using bremsstrahlung and power law models (the reader is referred to that paper for more details).

Of the 15 sources identified by RPS97, 12 fall within the same field of view as our VLA images at 6 and 20 cm (as

TABLE 4

POSITIONS AND LUMINOSITIES OF X-RAY SOURCES IN NGC 300[a]

Source Number	R.A. (J2000.0)	Decl. (J2000.0)	Net Counts[b]	log $L_{\rm Total}$ (ergs s^{-1}) (0.1–2.0 keV)
1.....	00 54 31.73	−37 38 16.4	37.1 ± 9.0	36.17
2.....	00 54 37.67	−37 42 42.7	44.8 ± 9.7	36.35
4.....	00 54 40.85	−37 40 40.6	86.5 ± 12	36.66
5.....	00 54 45.07	−37 41 32.5	106 ± 13	36.56
6.....	00 54 50.13	−37 38 42.7	43.6 ± 9.4	36.45
7.....	00 55 09.80	−37 42 06.5	921 ± 33	37.75
8.....	00 55 10.66	−37 48 26.9	280 ± 19	37.21
9.....	00 55 10.72	−37 38 49.7	204 ± 17	37.32
10	00 55 15.57	−37 44 33.5	53.4 ± 10	36.50
11	00 55 20.60	−37 48 10.3	112 ± 13	36.57
12	00 55 26.52	−37 38 32.3	38.3 ± 9.3	36.22
13	00 55 27.14	−37 36 47.0	47.4 ± 9.9	36.39

[a] Taken from the list provided in RPS97. Sources 3, 14, and 15 from that list fall outside the field of the VLA images and will not be considered here.
[b] In the total energy band.

discussed in § 2.1): the remaining three sources (3, 14, and 15 in the notation of RPS97) will not be considered here. The X-ray emission from NGC 300 (corresponding to the "total" X-ray band) is shown in contours in Figure 1, with Hα emission from this galaxy depicted in gray scale. We present characteristics of these X-ray sources in Tables 4 and 5: source number, position, net counts, and luminosity in the total band are given in the former table, while the results of the spectral fits and counterparts in the optical and radio are presented in the latter. We have confirmed at the 3 σ level or higher the presence of each of the sources given by RPS97, and we quote the properties (e.g., position, number of counts, and spectral fit) given for these sources by those authors. We have not found any new sources in addition to those found by RPS97. The X-ray sources shown in these tables were used to form an X-ray–selected sample of SNR candidates, as described in § 5.

3. MULTIWAVELENGTH PROPERTIES OF THE OPTICALLY SELECTED SNRS

Positional coincidences at the three wavelengths bands were sought in the following manner: a coincidence was considered possible between a PSPC X-ray source and an optical source, as well as a PSPC X-ray source and a radio source, if the offset between the two sources did not exceed $\sim 30''$, the approximate width of the PSPC point-spread function. For comparisons between radio and optical sources, a coincidence was considered to be real if the offset did not exceed $\sim 5''$, the approximate resolution of the radio images.

We found that the majority of the 28 optically identified SNRs had no detectable X-ray or radio emission to a 3 σ detection limit of 1.5×10^{36} ergs s^{-1} in X-ray luminosity, 0.1 mJy at 6 cm, and 0.2 mJy at 20 cm. Only two SNRs,

TABLE 5

SPECTRAL FITS AND COUNTERPARTS (OPTICAL AND RADIO) OF X-RAY SOURCES IN NGC 300[a]

	Spectral Fits[b]				
	Bremsstrahlung		Power Law		
Source Number	Column (10^{20} cm^{-2})	Temperature (keV)	Column (10^{20} cm^{-2})	Index	Optical/Radio Counterparts
1.....	$16.9^{+47.4}_{-16.9}$	$0.58^{+1.77}_{-0.48}$	(33.8)	(4.13)	D29
2.....	$20.3^{+33.4}_{-20.3}$	$1.29^{+8.58}_{-1.29}$	(28.5)	(2.64)	D40, R2
4.....	$82.8^{+9.78}_{-24.6}$	$0.10^{+0.03}_{-0.10}$	...	...	N300-S10 (DDB 2)
5.....	$70.1^{+28.5}_{-36.2}$	$0.13^{+0.08}_{-0.05}$	...	...	Uncataloged H II region, R5
6.....	(42.5)	(10.0)	$33.9^{+65.1}_{-33.9}$	$1.02^{+2.51}_{-1.02}$	...
7.....	...	(0.71)	$7.88^{+0.71}_{-0.68}$	$2.96^{+0.16}_{-0.16}$	...
8.....	...	(0.80)	$11.3^{+3.72}_{-2.36}$	$2.91^{+0.37}_{-0.32}$	...
9.....	$8.40^{+0.54}_{-0.55}$	$0.10^{+0.05}_{-0.10}$	...	...	...
10	$6.98^{+17.6}_{-3.2}$	$0.51^{+0.45}_{-0.29}$	(11.2)	(3.25)	BL N300-S26 (DDB 5)
11	$1.33^{+0.92}_{-0.75}$	$0.57^{+0.27}_{-0.16}$	...	...	Uncataloged H II region
12	(0.32)	(10.1)	$0.00^{+2.28}_{-0.00}$	$1.12^{+0.70}_{-0.33}$	...
13	(6.18)	(10.0)	$4.02^{+23.4}_{-4.01}$	$1.09^{+1.38}_{-0.82}$	...

[a] Source identifications and parameters of spectral fits are taken directly from RPS97. The optical and radio counterpart identifications for these X-ray sources are made for the first time by the present paper.
[b] Parameters of fits are taken directly from RPS97. The parameters of the superior fit, bremmsstrahlung or power law, are listed in normal text, while the parameters of the other fit (where listed by those authors) are given in parenthesis.

denoted as N300-S10 and N300-S26, possess significant X-ray emission and nonthermal radio emission. Both of these SNRs possess remarkably high Hα surface brightnesses (on the order of 10^{-15} ergs cm^{-2} s^{-1} arcsec^{-2}) that are approximately an order of magnitude brighter than the average value for SNRs in this Galaxy as measured by BL97. A third SNR, N300-S11, shows significant nonthermal radio emission, but no X-ray emission. In Figures 2–4, we present figures comparing two different wavelengths for each of these particular optically identified SNRs. In each figure, Hα emission is shown in gray scale, while total band X-ray emission (as observed by the PSPC instrument), 6 cm emission and 20 cm emission are shown in contours in the upper left, upper right, and bottom figures, respectively. Spectral properties of these particular optically identified SNRs (the [S II]/Hα ratio and linear diameter as determined by BL97, flux densities at 6 and 20 cm and the spectral index α) are listed in Table 6.

N300-S10, which was first found by DDB80, represents the clearest case in our sample of the detection of an optically identified SNR in both the X-ray and radio at a 3 σ level. This source lies along the northern edge of the large H II region designated as Deharveng 45 (from the catalog of D88), which is part of a star formation complex found near the center of NGC 300. Although diffuse radio emission from Deharveng 45 makes it difficult to isolate the radio emission at both 6 and 20 cm, it was possible to obtain a rough estimate of the nonthermal emission from this source by estimating and subtracting the thermal contribution (see Table 6). The calculated spectral index for sources that are contaminated by such diffuse emission can only be given as lower limits, and the true indices may be even steeper.

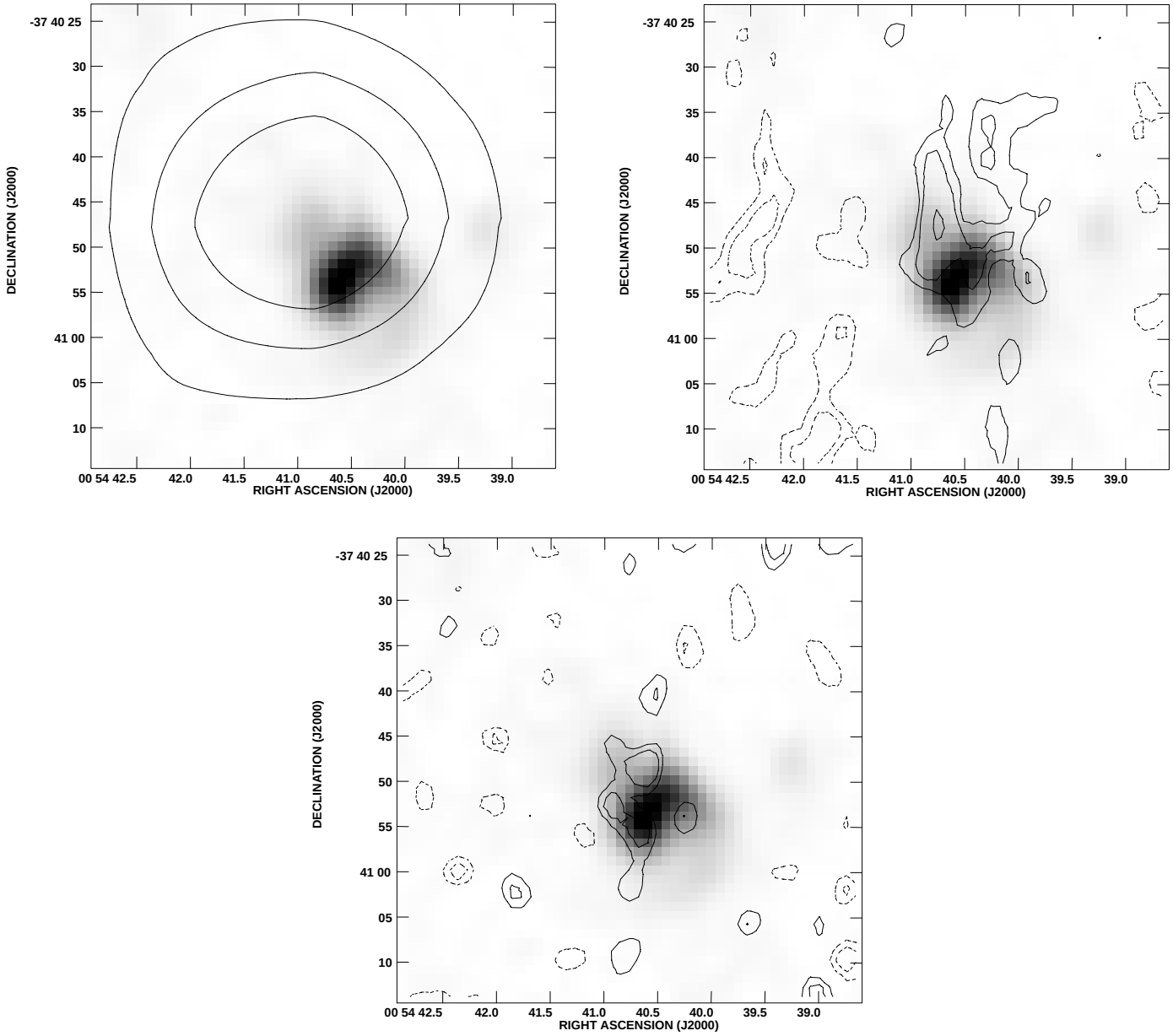

FIG. 2.—Multiwavelength images of the environment surrounding the optically identified SNR N300-S10. In each figure, the Hα emission is depicted in gray scale. X-ray emission (as observed by the PSPC instrument) is depicted in contours in Fig. 2*a* (*upper left*), using the same contour levels as in Figure 1. Emission at 6 cm and 20 cm is depicted in contours in Fig. 2*b* (*upper right*) and 2*c* (*bottom*), respectively. These contours are placed at −3, −2, 2, 3, 6, 9, 15, 30 and 60 times the base level (36 μJy in the 6 cm image and 60 μJy in the 20 cm image). The approximate beam sizes are ≈ 4″ and ≈ 6″ in the final 6 cm and 20 cm images, respectively. See § 3.

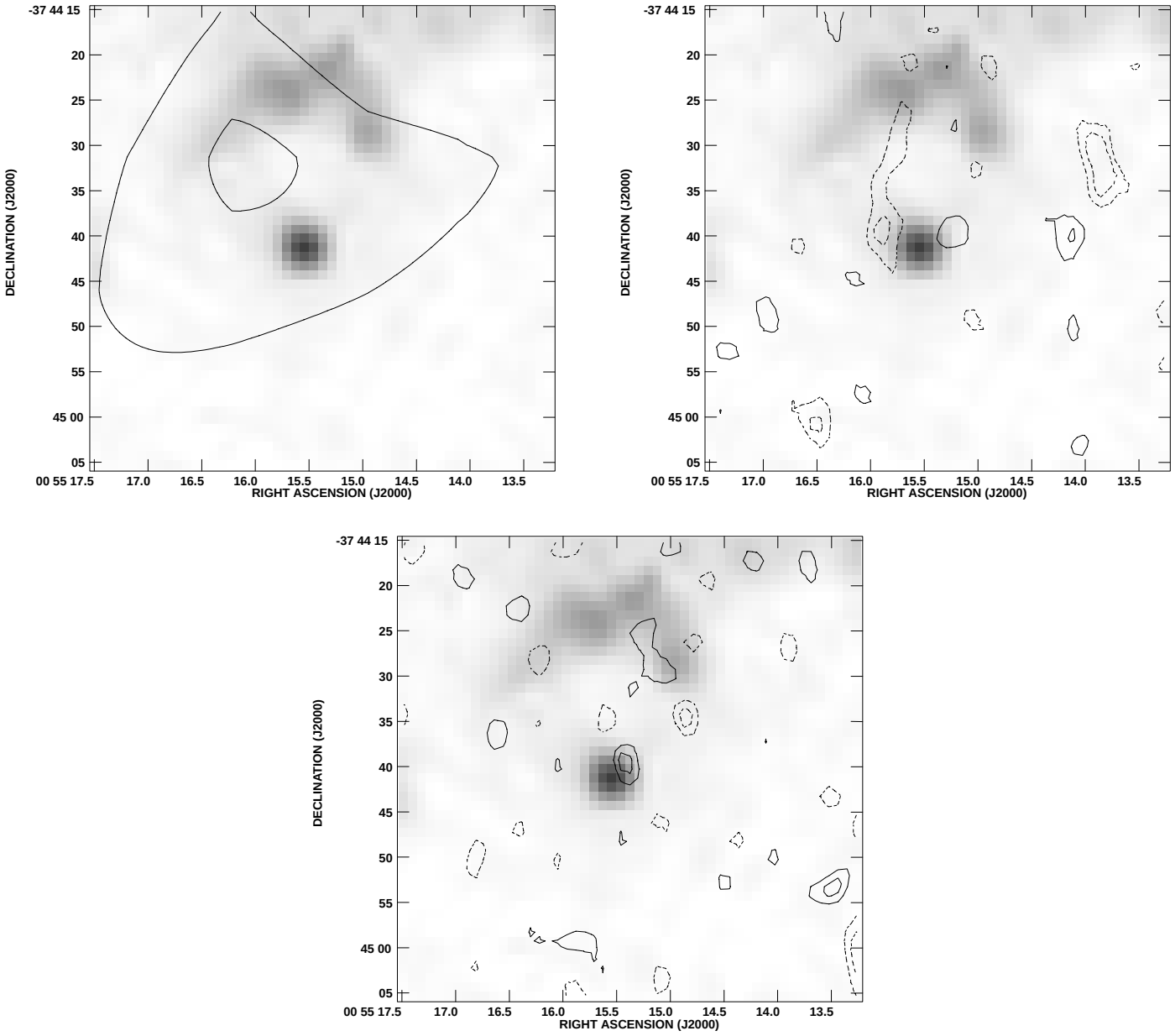

FIG. 3.—Same as Fig. 2, but for the optically identified SNR N300-S26

Inspection of the list of X-ray sources in this galaxy presented by RPS97 reveals that the X-ray source 4 is coincident with N300-S10. In addition, those authors determined a best-fit of the spectra of this source by using a thermal bremsstrahlung model characterized by an energy of $kT = 0.10^{+0.03}_{-0.10}$, which is consistent with the energy typical of a SNR. Likewise, N300-S26 (also first identified by DDB80) possesses both X-ray and radio emission at the 3 σ level, though in this case the radio emission is observed at the 3 σ level only at 20 cm. X-ray source 10 from the catalog of RPS97 is coincident with the optically identified SNR and the peak of the 20 cm emission, and like the X-ray source 4,

TABLE 6

SPECTRAL PROPERTIES OF OPTICALLY-IDENTIFIED SNRS IN NGC 300

Source Name	[S II]/Hα	Diameter (pc)	X-ray Emission?	S_6 (mJy)	δS_6 (mJy)	S_{20} (mJy)	δS_{20} (mJy)	α	δα
N300-S10	0.67	16	Yes	0.14[a]	0.04	0.29[a]	0.07	+0.6	0.3
N300-S11	0.66	43	No	0.39[a]	0.06	0.89[a]	0.15	+0.7	0.2
N300-S26	0.57	33	Yes	<	0.1	0.22	0.07	>0.7	...

[a] Diffuse radio emission from the adjacent H II region makes isolating the radio emission associated with the SNR difficult at this wavelength.

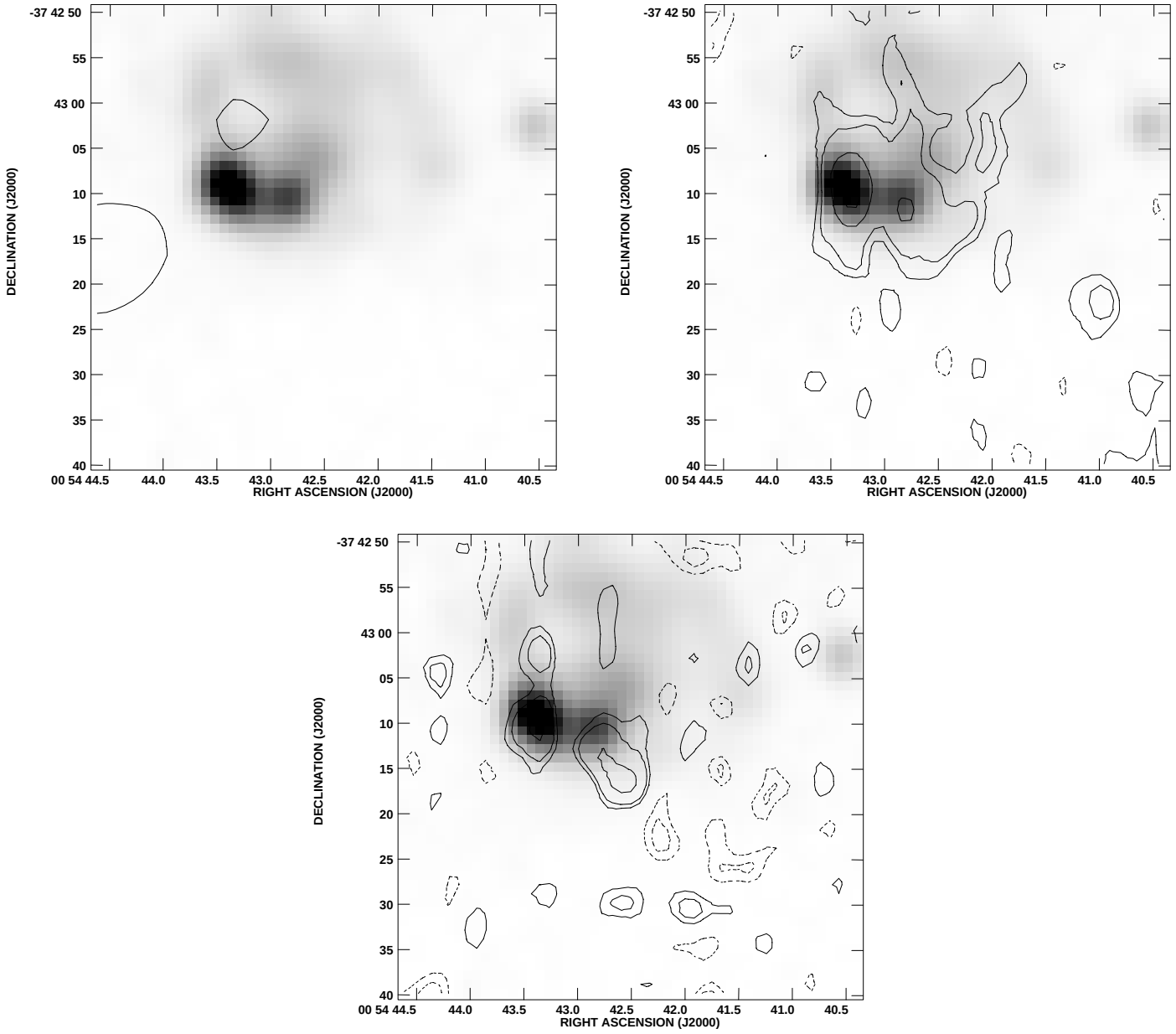

FIG. 4.—Same as Fig. 2, but for the optically identified SNR N300-S11

the spectrum of source 10 can be best fitted by a thermal bremmstrahlung model with an energy of less than 1 keV (the actual model parameter is $kT = 0.51^{+0.45}_{-0.29}$ keV), again consistent with the spectra expected for a SNR.

One other optically identified SNR possesses a radio counterpart, but not an X-ray counterpart. N300-S11, located just at the southwest edge of the H II region Deharveng 53, features very strong nonthermal radio emission, but diffuse radio emission from the H II region complicates the isolation of the radiation from the SNR. Inspection of the PSPC image indicates that a weak X-ray source (less than 3 σ) may be associated with this SNR, and the catalog of X-ray sources presented by RPS97 does not list a source at this position. We therefore conclude that there is no X-ray emission associated with this SNR, at least in the PSPC image, though further X-ray study will be needed to determine the true X-ray characteristics of this SNR.

We note that for the SNRs N300-S10 and N300-S26, BL97 found enhanced electron densities in the surrounding regions around both of these remnants. These authors suggest that N300-S26 is expanding into a high-density preshock material with an electron density n_e of $10 - 20$ cm^{-3}. We also note that these two SNRs have two of the smallest diameters of the SNRs found in this galaxy by BL97. In § 6, we will discuss the spectral properties of these SNRs together with the other candidate SNRs found in this survey at the other wavelengths.

4. PROPERTIES OF THE RADIO-SELECTED SNR CANDIDATES

Isolated SNRs for which [S II]/H$\alpha \leq 0.4$ (known as Balmer-dominated SNRs) are typically missed by optical surveys such as those by DDB80 and BL97. Prominent examples of Balmer-dominated SNRs in our own Galaxy include SN 1006 and Tycho's SNR (3C 10) (Smith 1997).

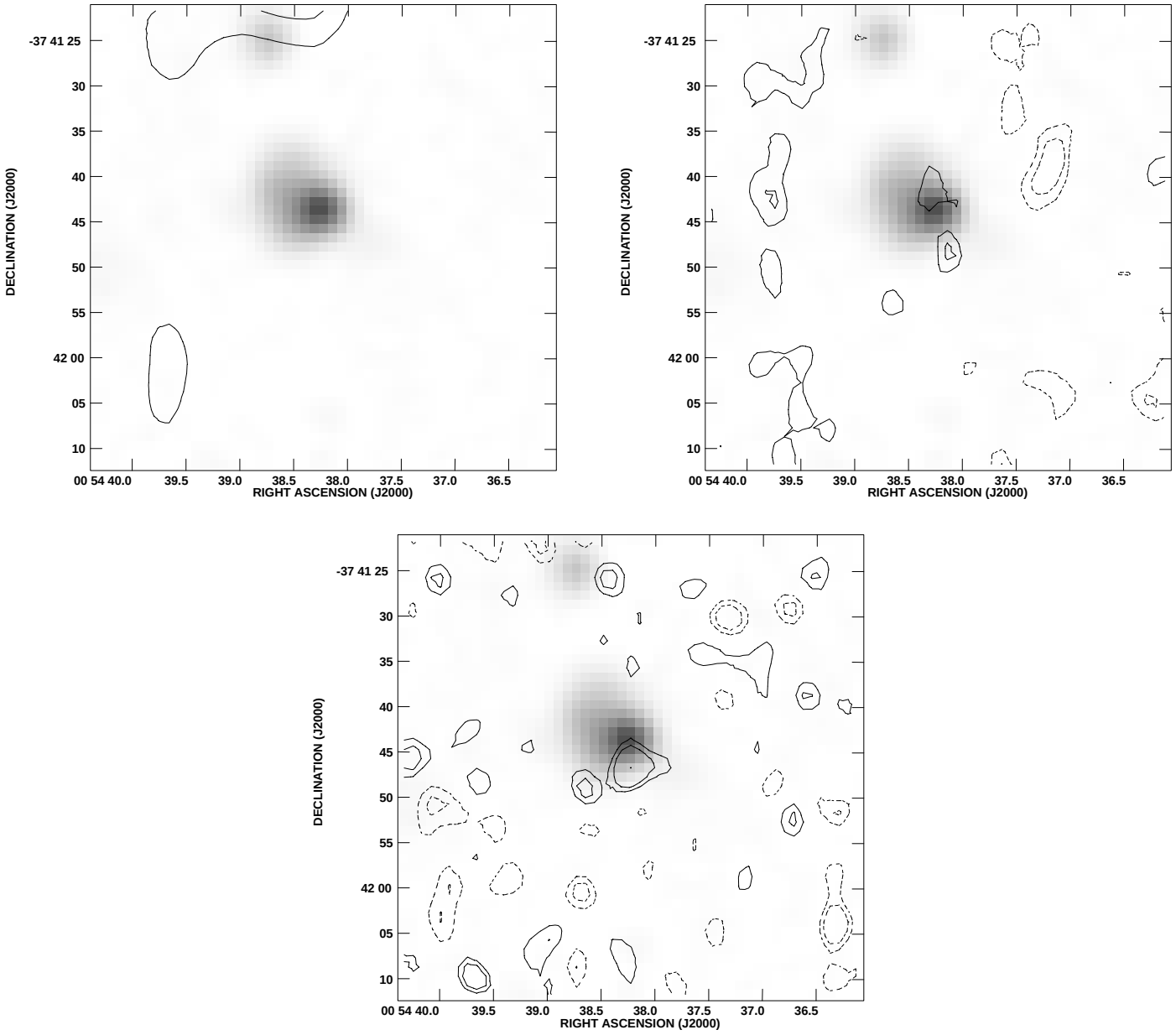

FIG. 5.—Same as Fig. 2, but for the candidate radio SNR R1 in the H II region Deharveng 39

Furthermore, even those SNRs that are not Balmer-dominated may be missed by optical surveys if the SNRs are located near or in bright H II regions. A good example of such an SNR can be found in the study by Gordon et al. (1993): these authors combined X-ray, optical, and radio observations to identify a SNR embedded in the giant H II region NGC 592 in the galaxy M33. Thus, nonthermal radio sources associated with regions of Hα emission may

TABLE 7

FLUX DENSITIES OF NGC 300 SNRS AND SELECTED GALACTIC SNRS, NORMALIZED TO THE CAS A DISTANCE ($d \sim 3.4$ kpc)[a]

SNR	S_{20} (Jy)	SNR	S_{20} (Jy)	SNR	S_{20} (Jy)	SNR	S_{20} (Jy)
Cas A	*2720*	R13	191	R11	134	R5.....	88
W28	*377*	*Kes 79*.....	*190*	R6.....	114	R7.....	84
Crab	*360*	R10	183	R8.....	114	N300-S26.....	84
N300-S11.....	340	*W44*	*179*	N300-S10.....	111	*Puppis A*	*54*
W49B.....	*329*	R12	160	R14	107	*Vela*.....	*38*
R2.....	229	*3C 391*.....	150	R9.....	92	*IC 443*	*31*
R3.....	217	R1	137	R4.....	92		

[a] Galactic SNRs are listed in italics, while NGC 300 SNRs found in this paper are listed in regular font.

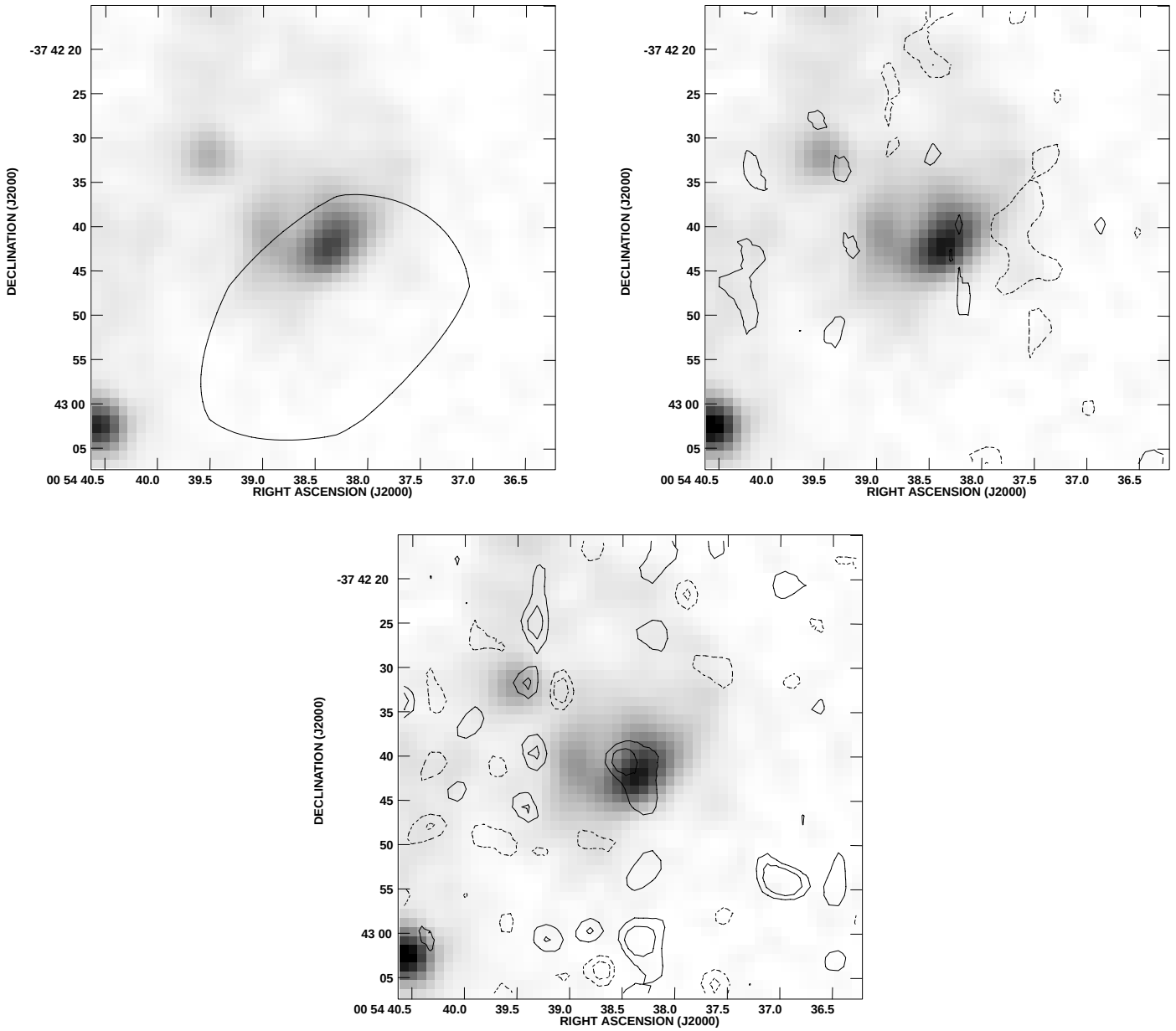

FIG. 6.—Same as Fig. 2, but for the candidate radio SNR R2 in the H II region Deharveng 40

be considered excellent candidate radio SNRs. In order to identify a radio source as a SNR candidate we imposed three criteria: (1) the radio source must be detected at a 3 σ level at 20 cm, (2) a corresponding 6 cm radio source should have a flux density or an upper limit that is consistent with a nonthermal spectrum, and (3) the radio source must be associated with a region of Hα emission. The third criterion introduces an obvious selection effect against radio SNRs that lack optical counterparts; this criterion is necessary in order to differentiate background radio sources from sources intrinsic to NGC 300. Based on the estimates of Mitchell & Condon (1985) for the number density of background sources, we estimate that approximately five background sources should be observed in random directions through the disk of NGC 300 in the 20 cm image at a 3 σ level of 0.2 mJy or greater.

To investigate the issue of background source confusion further, we searched for position coincidences between regions of Hα emission and "negative" sources that registered at the -3 σ level and found only one such coincidence. This result is consistent with the expected number of random superpositions of background sources seen through the disk of NGC 300 on H II regions located in that galaxy. Although these criteria select against isolated radio-emitting SNRs, SNRs embedded in H II regions can be detected. Thus, an estimate on the SNR population missed in optical surveys can be derived.

Using the above criteria, we have found 17 nonthermal radio sources associated with regions of Hα emission and list the properties of these sources (coordinates, flux densities at 6 and 20 cm, spectral indices and associated H II region) in Table 3. We concentrated our efforts on the regions of Hα emission listed in the catalog given by D88, but also considered bright regions that were not included in that paper (for example, the region associated with our radio source R5). Of these 17 nonthermal radio sources, 14

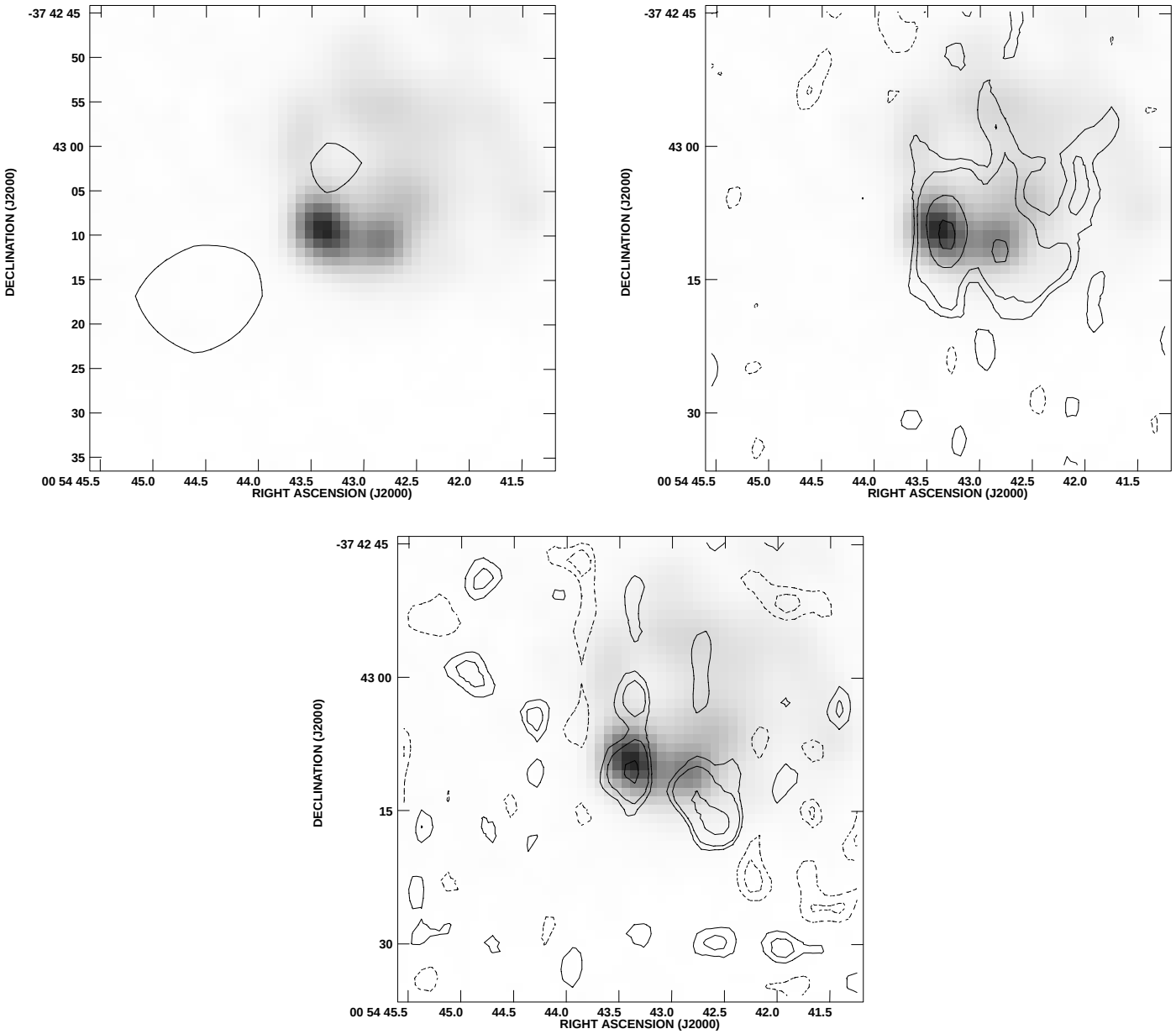

FIG. 7.—Same as Fig. 2 but for the candidate radio SNR R3 in the H II region Deharveng 53A

are new candidates, while the other three sources were already identified in the optical sample and were discussed in § 3. In the cases where no detectable emission was found for the SNR at 6 cm, we have calculated a lower limit to the spectral index of the source. In the final column of Table 3, we present the identification of the H II region (from the catalog of D88) associated with each radio source. In Figures 5–18, we show images of the new candidate radio SNRs.

As an additional check on the false alarm rate we performed two statistical tests on the radio-selected sample of SNRs. First, we compared the radio emission of the SNR candidates in NGC 300 with well-known Galactic SNRs. The comparison is summarized in Table 7 where the 20 cm flux densities of 10 well-studied Galactic SNRs (taken from D. A. Green[3]) are compared with the NGC 300 candidates. All flux densities are normalized to the distance to Cas A (3.4 kpc, Reed et al 1995). The sensitivity limit of 0.2 mJy for sources in NGC 300 translates into a threshold detection of a SNR with a flux density of 76 Jy at the Cas A distance. While none of the NGC 300 SNRs are the equivalent of the most luminous Galactic SNR, Cas A, their flux densities are generally quite comparable to Galactic SNRs.

Secondly, we draw a direct comparison with the equidistant sample of SNRs in M33 (Duric et al. 1995), a galaxy

[3] See D. A. Green, A Catalogue of Galactic Supernova Remnants (1998 September version; Cambridge: Mullard Radio Astronomy Observatory), available on the World Wide Web at http://www.mrao.cam.ac.uk/surveys/snrs/.

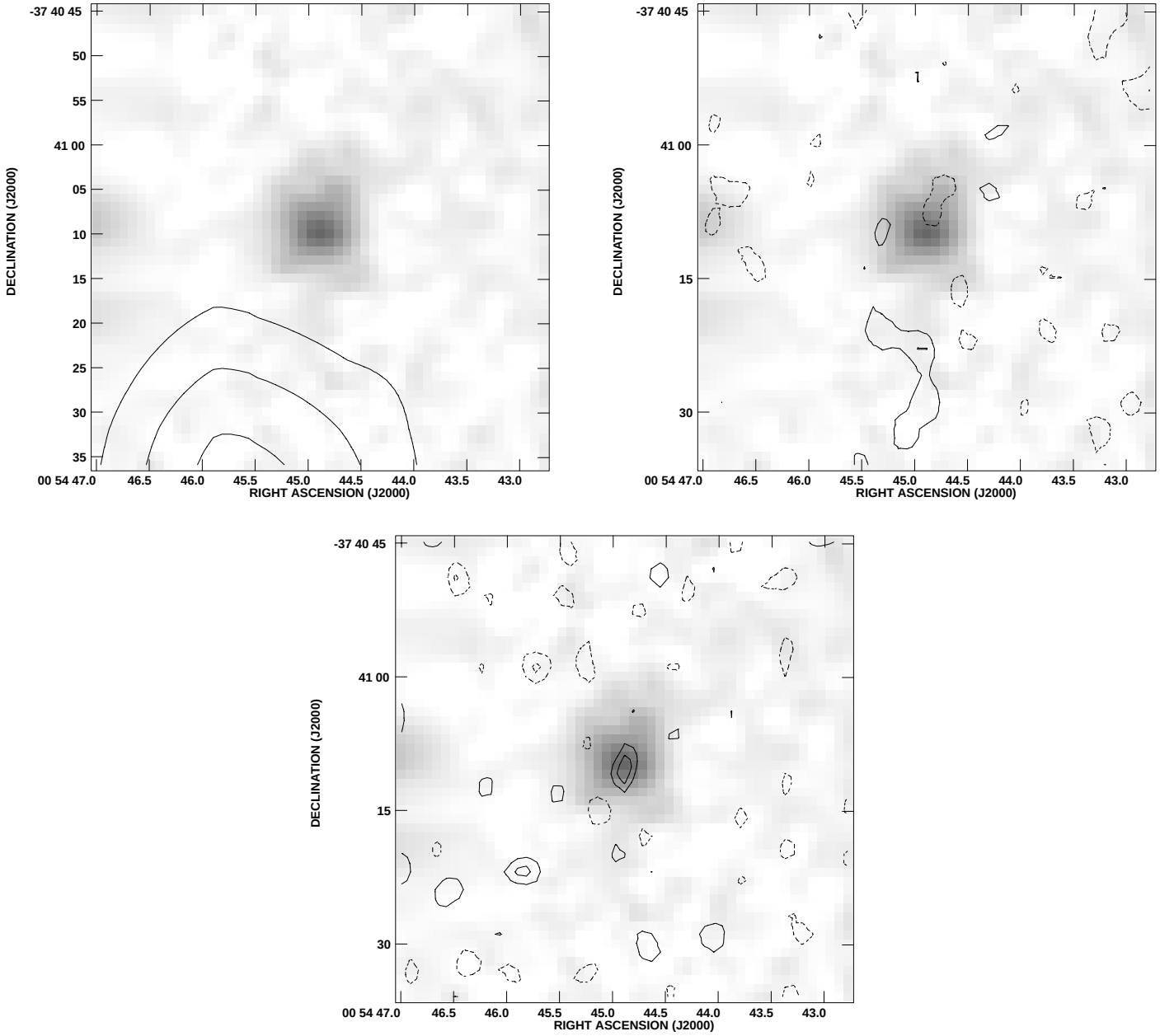

FIG. 8.—Same as Fig. 2, but for the candidate radio SNR R4 in the H II region Deharveng 60

with many similarities to NGC 300. If we scale the 3 σ sensitivity limit at 20 cm of 0.2 mJy to the distance of M33 (840 kpc; Freedman, Wilson, & Madore 1991), the corresponding flux density is approximately 1.2 mJy. Of the 53 radio-emitting SNRs found by Duric et al. (1995) in M33, 13 have flux densities that exceed 1.2 mJy. This number is comparable to the 17 candidate radio SNRs found in our survey of NGC 300.

We conclude that the flux densities of the radio-selected SNR candidates are consistent with both Galactic SNRs and SNRs found in M33. These similarities strengthen the case that the radio-selected candidates are indeed SNRs.

5. PROPERTIES OF THE X-RAY–SELECTED SNR CANDIDATES

To complete our search for SNRs in NGC 300, we examined the X-ray sources listed in Tables 4 and 5 and discussed in § 2.3. To determine if any of these sources may be considered viable candidate SNRs, the following selection criteria were used: (1) the source spectrum is soft and (2) the source has an Hα counterpart to within the positional uncertainty of the PSPC point-spread function. The sources which satisfy these criteria were sources 1, 2, 4, 5, 9, 10, and 11: each one of these sources had a derived temperature of less than 1 keV, or (in the case of source 2) the error bounds on the determined temperature permitted a value of less than 1 keV. The sources 4 and 10 have already been discussed in association with optically identified SNRs in § 3.

While source 9 also possesses a soft spectrum, inspection of its emission in the two separate pointings of 37 and 9.3 ks indicates a possible time variability in its X-ray luminosity. In addition, there is an extended component to this source that is not consistent with the compact emission expected from a SNR at this distance. On the basis of these two

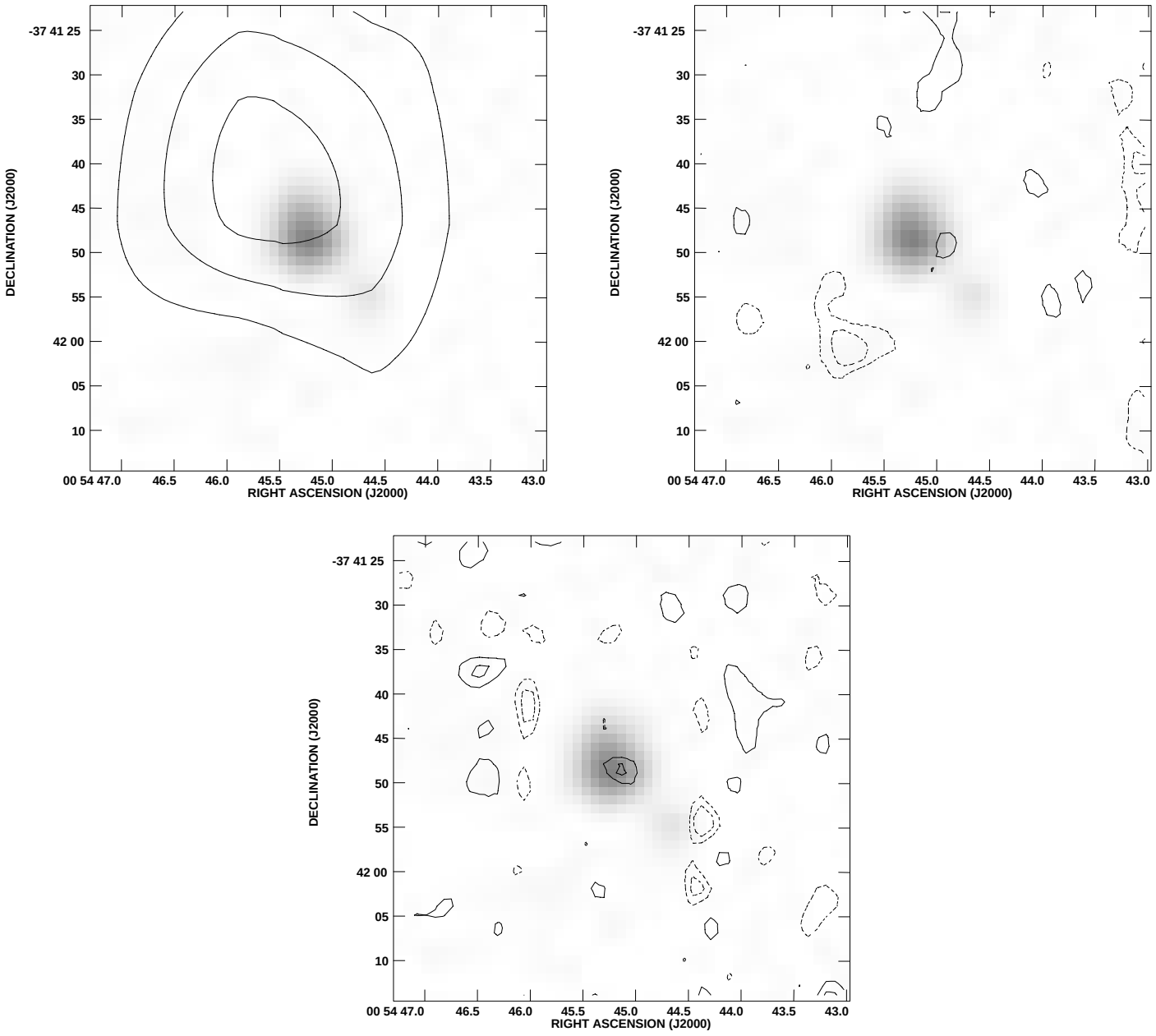

FIG. 9.—Same as Fig. 2, but for the candidate radio SNR R5 in an uncataloged H II region

properties of the source, we do not include source 9 among the candidate X-ray SNRs. We note that it is possible that some of the other candidate X-ray SNRs may in fact actually be time-variable sources (such as X-ray binaries) with periods longer than the integration time of the observations, which would also preclude them from being classified as X-ray SNRs. However, such variability would not be detectable with the current data, and further observations of these sources will be needed to investigate their possible variability in more detail.

Of the remaining candidate X-ray SNRs, we find that two (2 and 5) are coincident with candidate radio SNRs (R2 and R4, respectively): these associations enhance the likelihood that these sources of X-ray emission are really associated with SNRs. The remaining two X-ray sources—1 and 11—are coincident with H II regions (Deharveng 29 and an uncataloged H II region, respectively): while no radio emission is detected from either of these sources, we believe that the soft-spectrum nature of both X-ray sources and their associations with H II regions indicates that both sources may be considered candidate SNRs.

In their study of discrete X-ray sources within M33, Long et al. (1996) analyzed the spectra of the individual X-ray sources by comparing the number of counts received in the hard and soft energy bands (see § 2.3). They found that the X-ray sources associated with optically identified SNRs generally possessed a soft spectrum. Our parallel study of the archived X-ray data using the method of Long et al. (1996) confirmed the results of RSP97.

In summary, the X-ray–selected sample of SNRs has yielded six candidate sources, of which two are in common with the optically selected sample and two more are in common with the radio-selected sample. The remaining two are new candidates, and the total number of new candidate

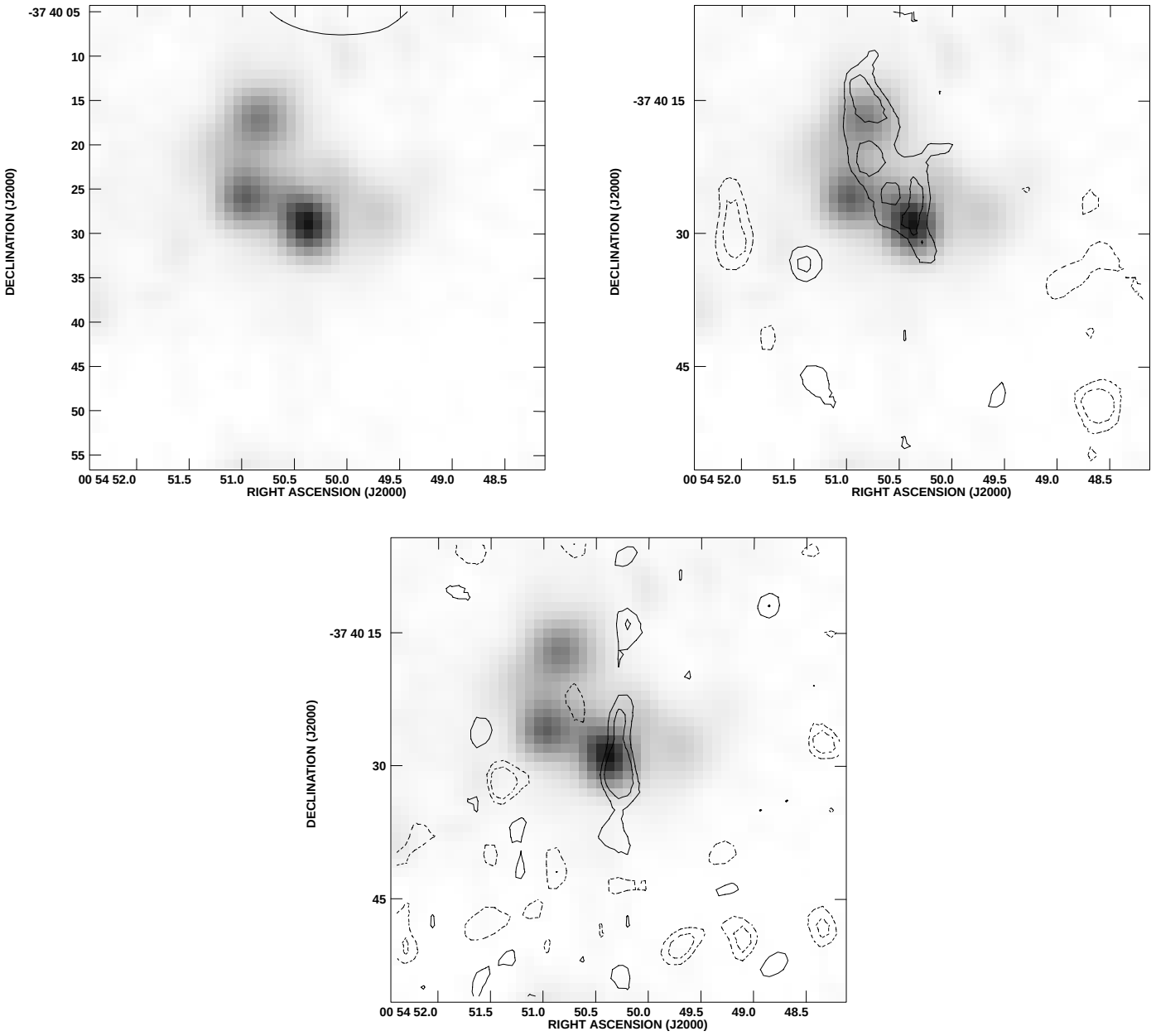

FIG. 10.—Same as Fig. 2, but for the candidate radio SNR R6 in the H II region Deharveng 76A

SNRs found in this galaxy is therefore raised to 16. The total number of candidate SNRs in this galaxy, including the 28 found by BL97, has been increased to 44.

6. DISCUSSION

6.1. *Comparison of the SNR Data Sets*

In Figure 19*a* we present a Venn diagram that depicts the results of our SNR search by showing the independent sets of SNR candidates selected at X-ray, radio and optical wavelengths. A Venn diagram for the SNRs in M33 is shown in Figure 19*b* for comparison, based on the sample of SNRs identified at the optical, radio, and X-ray wavelengths by Gordon et al. (1998), Duric et al. (1995), and Long et al. (1996), respectively. The most striking result for NGC 300 is the very limited intersection between the data sets. In particular, we note that very few of the optically identified SNRs possess counterparts at either X-ray or radio wavelengths, and only six of the entire set of 44 candidate SNRs have counterparts at other wavelengths. In M33 the intersection set is somewhat larger between the radio and optical data sets. While differences in sensitivity limits between the X-ray, radio and optical surveys must play an important role in populating the Venn diagram for a single galaxy, it is instructive to examine differences between galaxies for a given set of survey limits. Table 8 summarizes the sensitivity limits of the X-ray, radio, and optical surveys of M33 and NGC 300. It is clear that the survey limits are quite similar both in absolute terms and in relative terms. Apart from the fact that the total number of detected SNRs varies with distance, any other major differences between the M33 and NGC 300 Venn diagrams are more likely to be driven by distance effects.

We hypothesize that the limited overlap between the optical, X-ray and radio-selected samples of SNR candidates in NGC 300 relative to M33 may be the result of

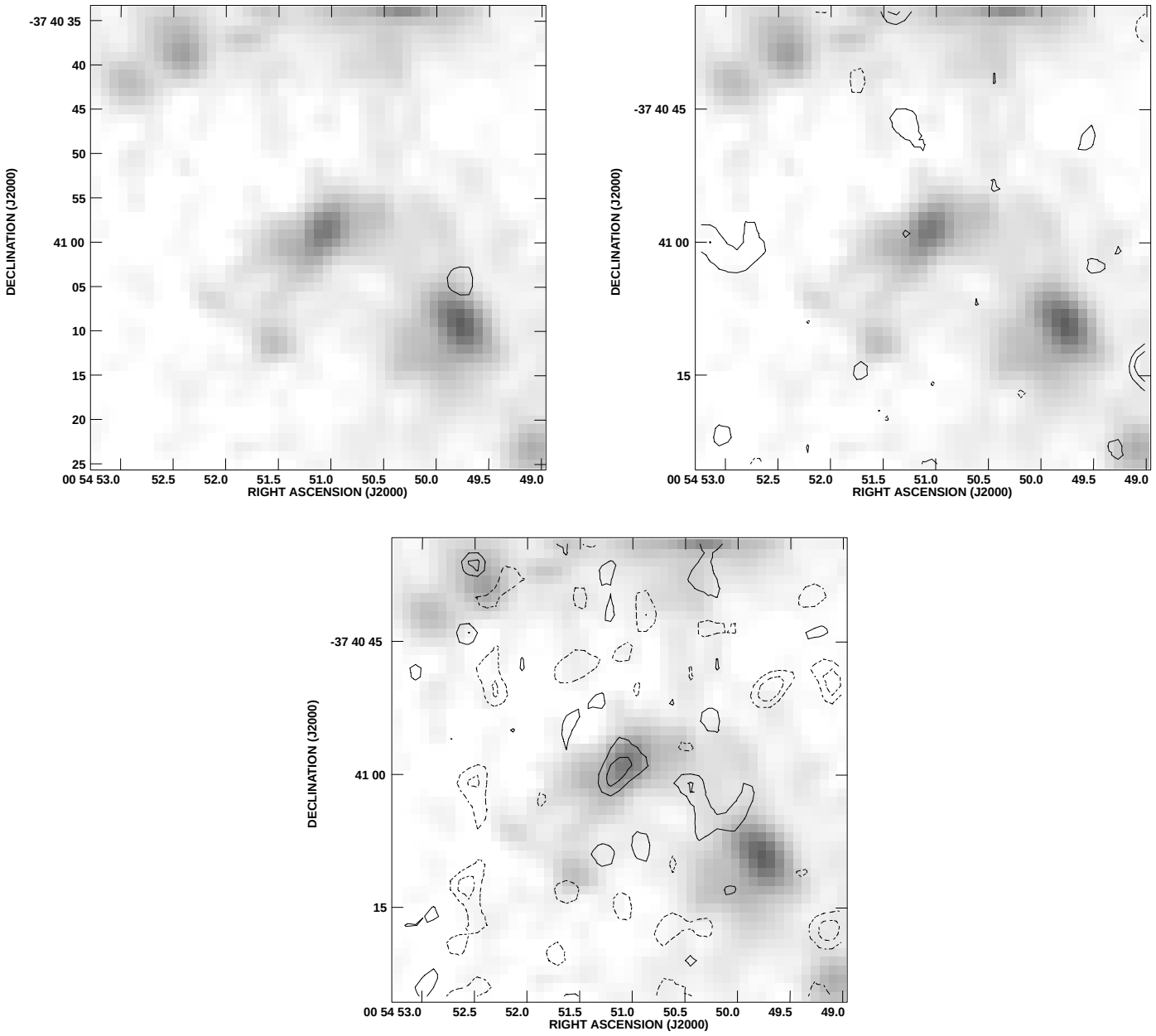

FIG. 11.—Same as Fig. 2, but for the candidate radio SNR R7 in the H II region Deharveng 80

competing distance-dependent selection effects. We now present a quantitative analysis of these effects.

6.2. *Analysis of Distance-dependent Selection Effects*

To investigate the issue of confusion in more detail, we performed the following experiment with our Hα image of NGC 300. A duplicate of this image was prepared where all of the Hα sources were reduced to one-tenth of their original fluxes while retaining the same background noise level. This second image (hereafter referred to as the "mock-[S II]" image) was intended to simulate a [S II] image of the galaxy. We then added twelve "artificial" SNRs to the original Hα image and the mock-[S II] image in the form of 5″ Gaussians with fluxes consistent with those expected for SNRs (namely, with the flux ratio of [S II]/Hα ≥ 0.6) and normalized to the average Hα flux of the SNRs found by

TABLE 8

SENSITIVITIES OF SURVEYS OF M33 AND NGC 300[a]

Galaxy	X-ray (count s^{-1})	Reference	Hα (ergs $cm^{-2}s^{-1}$ $arcsec^{-2}$)	Reference	20 cm (μJy $beam^{-1}$)	Reference
M33.....	5×10^{-4}	1	$\sim 6 \times 10^{-17}$	2	50	3
NGC 300.....	8×10^{-4}	4	$\sim 1 \times 10^{-16}$	5	60	6

[a] References: (1) Long et al. 1996, (2) Gordon et al. 1998, (3) Duric et al. 1995, (4) RPS97, (5) BL97, (6) this paper.

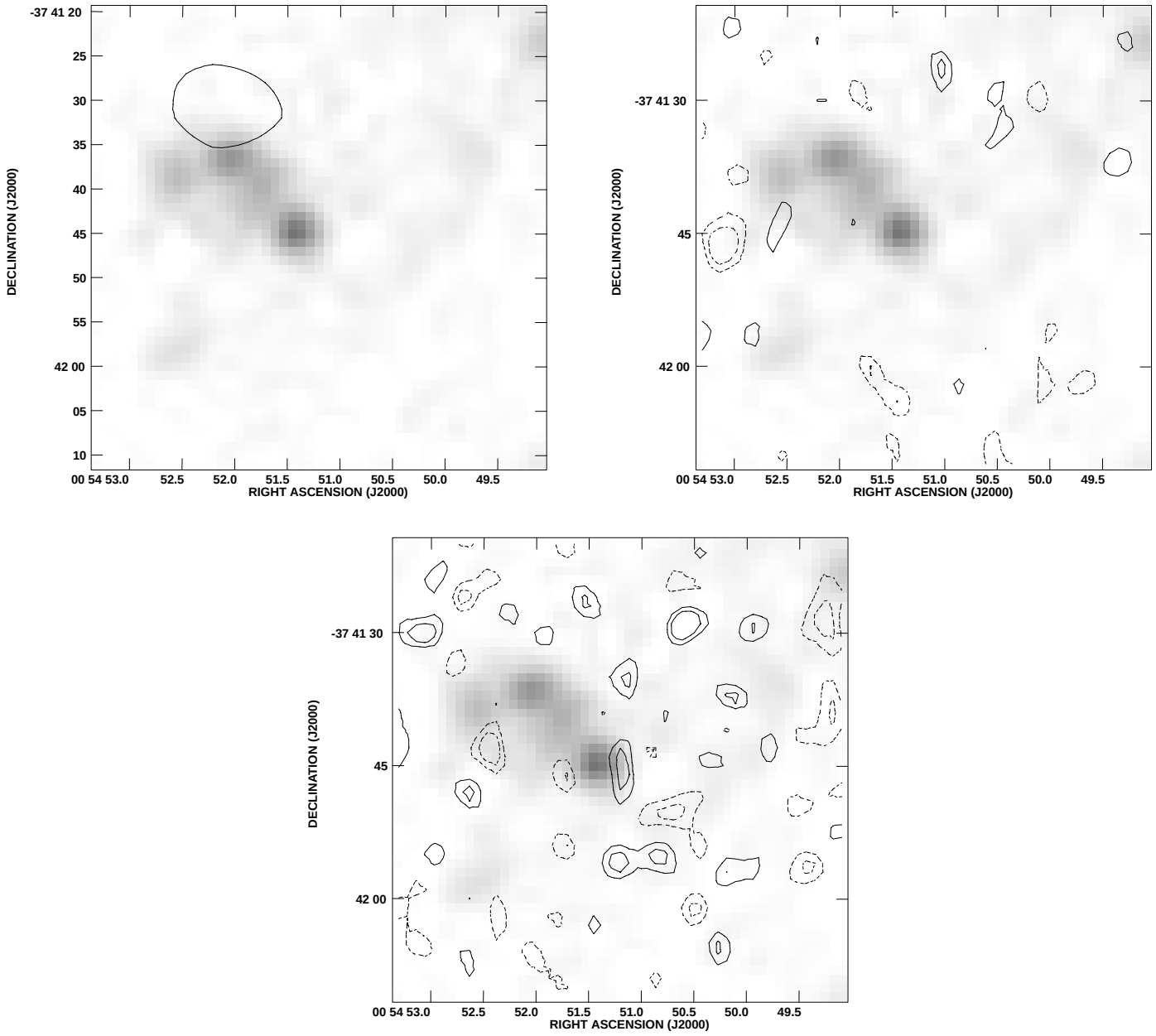

FIG. 12.—Same as Fig. 2, but for the candidate radio SNR R8 in the H II region Deharveng 81

BL97. The artificial SNRs were placed in a variety of environments to reproduce a variety of confusion effects: four of these sources (the "isolated" artificial SNRs, which we will denote as sources I1–I4) were placed in locations well away from Hα emission. Four more sources (the "perimeter" artificial SNRs, which we will denote as sources P1–P4) were placed along the perimeters of regions of Hα emission. Finally, the remaining four sources (the "embedded" artificial SNRs, which we will denote as sources E1–E4) were placed right inside regions of Hα emission.

The purpose of the simulation was to use the standard detection criterion (namely, the [S II]/Hα criterion) to attempt to detect the artificial SNRs. Four data sets were generated, with the original image and the mock-[S II] image forming the baseline pair. Three more data pairs were generated by smoothing the Hα and mock-[S II] images with 3″, 6″ and 9″ Gaussian point-spread functions. This smoothing was performed to mimic the effects of increasing distance to the galaxy. Since the baseline data pair is characterized by a point-spread function of $\sim 1''$, the other three data pairs represent increases in distance by a factor of 3, 6, and 9, respectively. The overall data set represents images of four galaxies spanning a factor of 9 range in distance, observed uniformly at the same angular resolution and to the same surface brightness level.

Ratio maps of [S II]/Hα were made for all four data pairs. We performed aperture photometry on the ratio maps at the expected positions of the artificial SNRs in order to determine the average values (that is, averaged over the angular size of the SNR) and the peak value (that is, the maximum pixel value in the aperture) of the ratio.

In Table 9 we present the results of our search for the artificial SNRs in each of the four prepared ratio images.

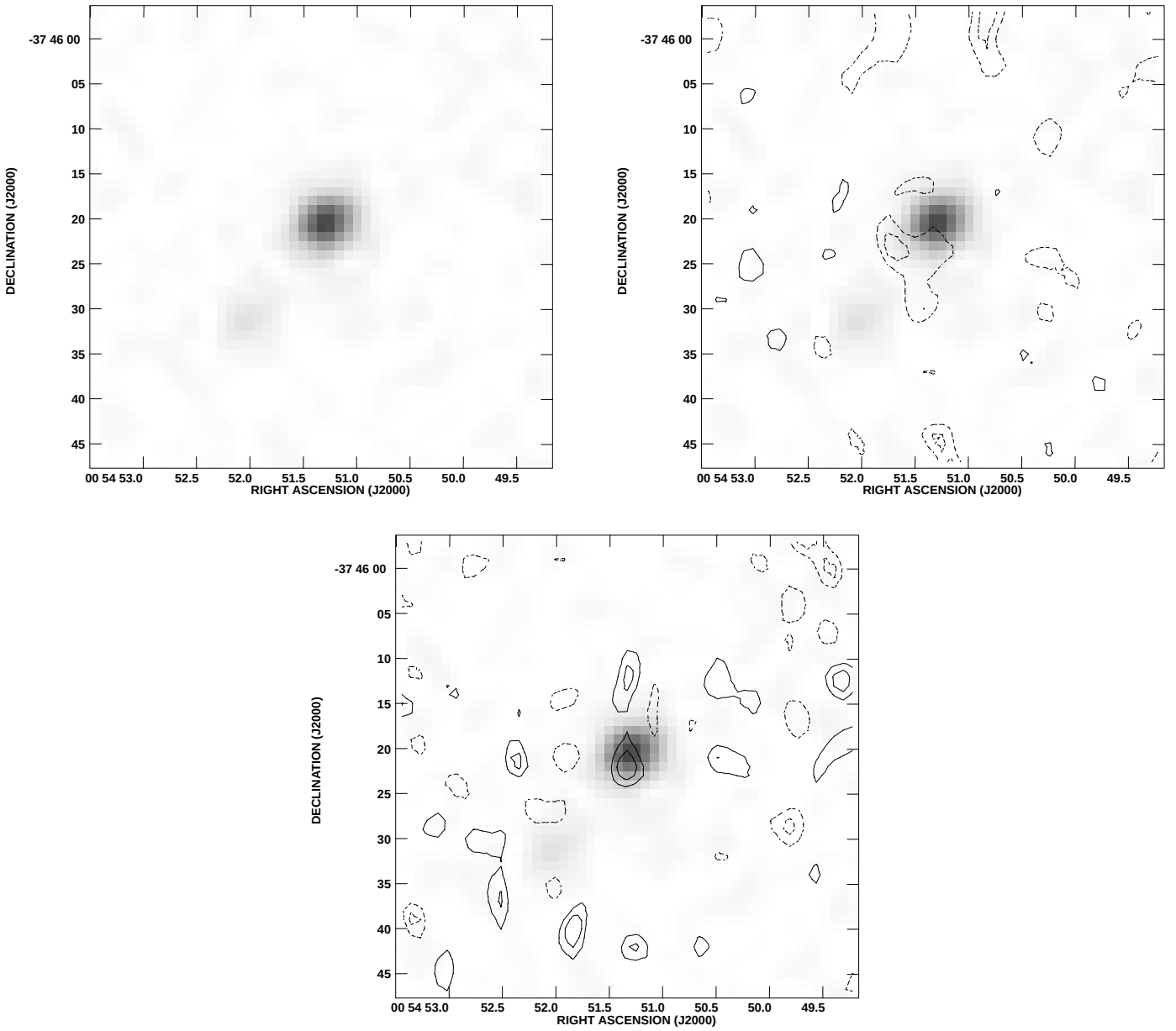

FIG. 13.—Same as Fig. 2, but for the candidate radio SNR R9 in the H II region Deharveng 82

We list the mean ratio value, the rms deviation, and the maximum ratio value in counts found in a $7'' \times 7''$ box centered on the position of each artificial SNR. If both the mean ratio value and the maximum ratio value exceeded 0.4, we considered the source detected, while if only one of these two quantities exceed that value, we considered the source possibly detected. If both of these values failed to exceed 0.4, we considered the source to be undetected.

Inspection of Table 9 reveals the following results:

1. Even in the baseline data set the embedded SNRs are not detected. The average surface brightness of the artificial SNRs is between 15 and 50 times larger than the surface brightnesses of the H II regions in which they are embedded. Consequently, the emission from the H II regions dilutes the ratio measurements to levels that fall below the detection threshold. We note that in the sample of optically identified SNRs given by BL97 the ratio of SNR surface brightness to that of H II regions fall in a similar range to that used in our simulation.

2. The detection of artificial SNRs becomes increasingly difficult with distance. Of the three perimeter SNRs that are at least possibly detected in the baseline ratio map, none are detected in the 9″ ratio map, which represents a factor of 9 increase in distance over the baseline map.

3. In the case of the four artificial SNRs that are completely isolated in the baseline ratio map, three are detected with full confidence in the 9″ map, while the remaining one is only possibly detected.

The above results clearly illustrated the effect of increasing galaxy distance on the detectability of SNRs using the [S II]/Hα method, namely that a bias favoring the detection of isolated SNRs becomes more pronounced as the distance to the galaxy increases. This effect may partially explain the difference in the SNR detections between M33 and NGC 300, where the latter galaxy is approximately 3 times more distant than the former, and therefore suffers from the effects we noted above.

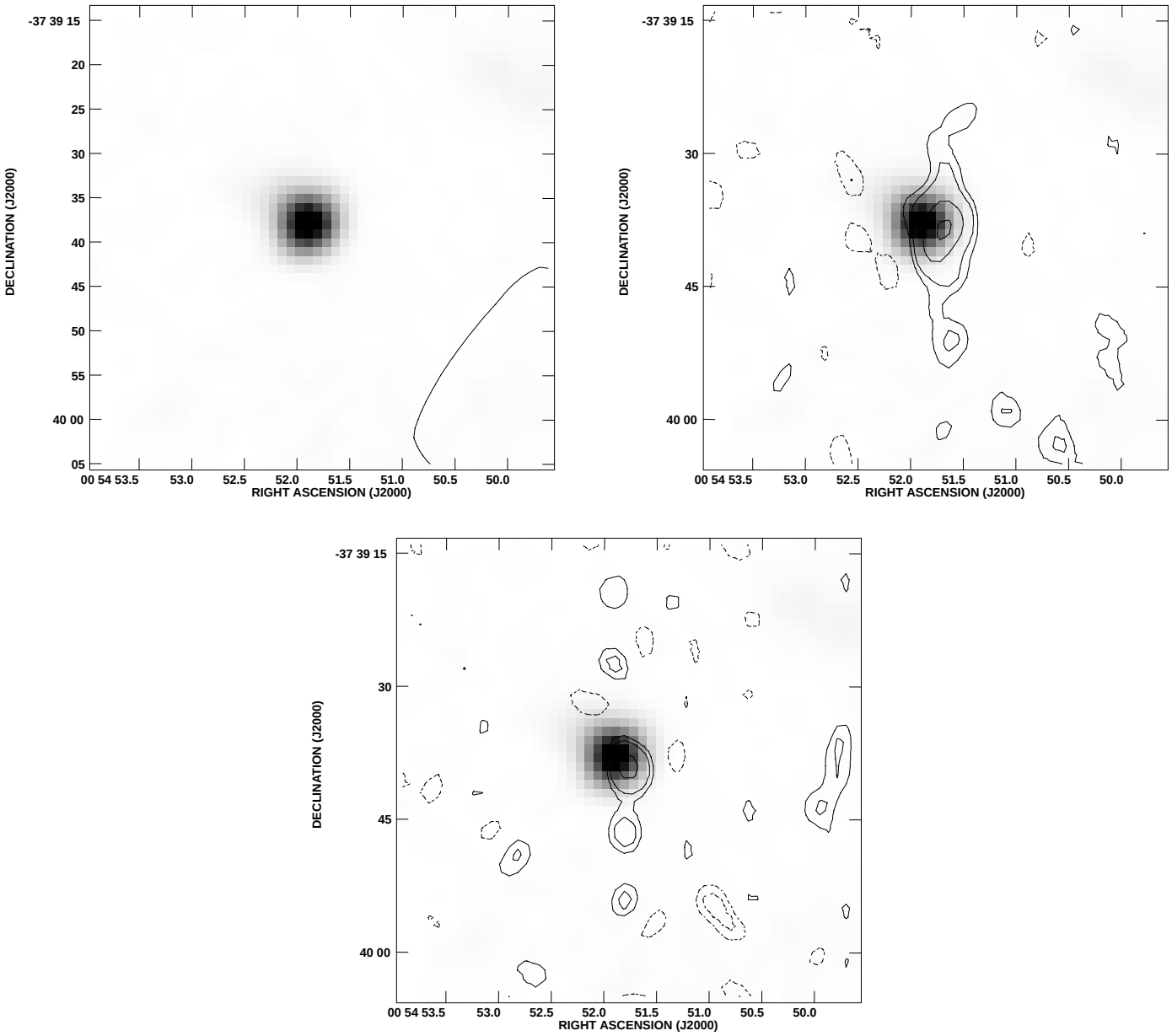

FIG. 14.—Same as Fig. 2, but for the candidate radio SNR R10 in the H II region Deharveng 84

Without specific knowledge of the luminosity function of embedded SNRs, it is difficult to conclusively "prove" our claim. However, given that luminosity functions favor fainter SNRs, in general, we expect the above effects to be even more severe for increasingly fainter SNRs. The results of our simulation are consistent with the hypothesis that distance-dependent confusion biases optically selected samples of SNRs to relatively isolated sources. If we further assume that the Hα surface brightness of an H II region is a measure of the gas density, then on average one could expect the embedded SNRs to be expanding into a denser medium relative to an isolated SNR. Evidence from X-ray observations of SNRs in M31 supports the notion that optically identified SNRs tend to lie in regions of low gas density (Magnier et al. 1997). Then, if the mechanism for the production of radio emission also depends on the density one would expect a relatively lower degree of correlation between the optically selected and radio-selected SNRs.

The obvious question to ask is why the radio data are not subject to these same effects. Since H II regions emit thermal bremsstrahlung (free-free radio emission), they play a similar confusing role. However, the major difference is that the free-free mechanism is inefficient relative to the synchrotron mechanism operating in the SNRs. In other words, the ratio of SNR radio surface brightness to that of the H II regions is sufficiently large, on average, that a greater proportion of the embedded population can be detected.

Figure 20 shows an artificial "perimeter" SNR as it appears in the [S II]/Hα ratio map. Note how the signal degrades as the galaxy is moved farther away.

6.3. *The Effect of Preshock Gas Density*

In general, SNRs detected by optical methods are biased toward regions of decreased confusion because SNRs are more difficult to detect in or near H II regions. It is even plausible that optical surveys are more likely to detect

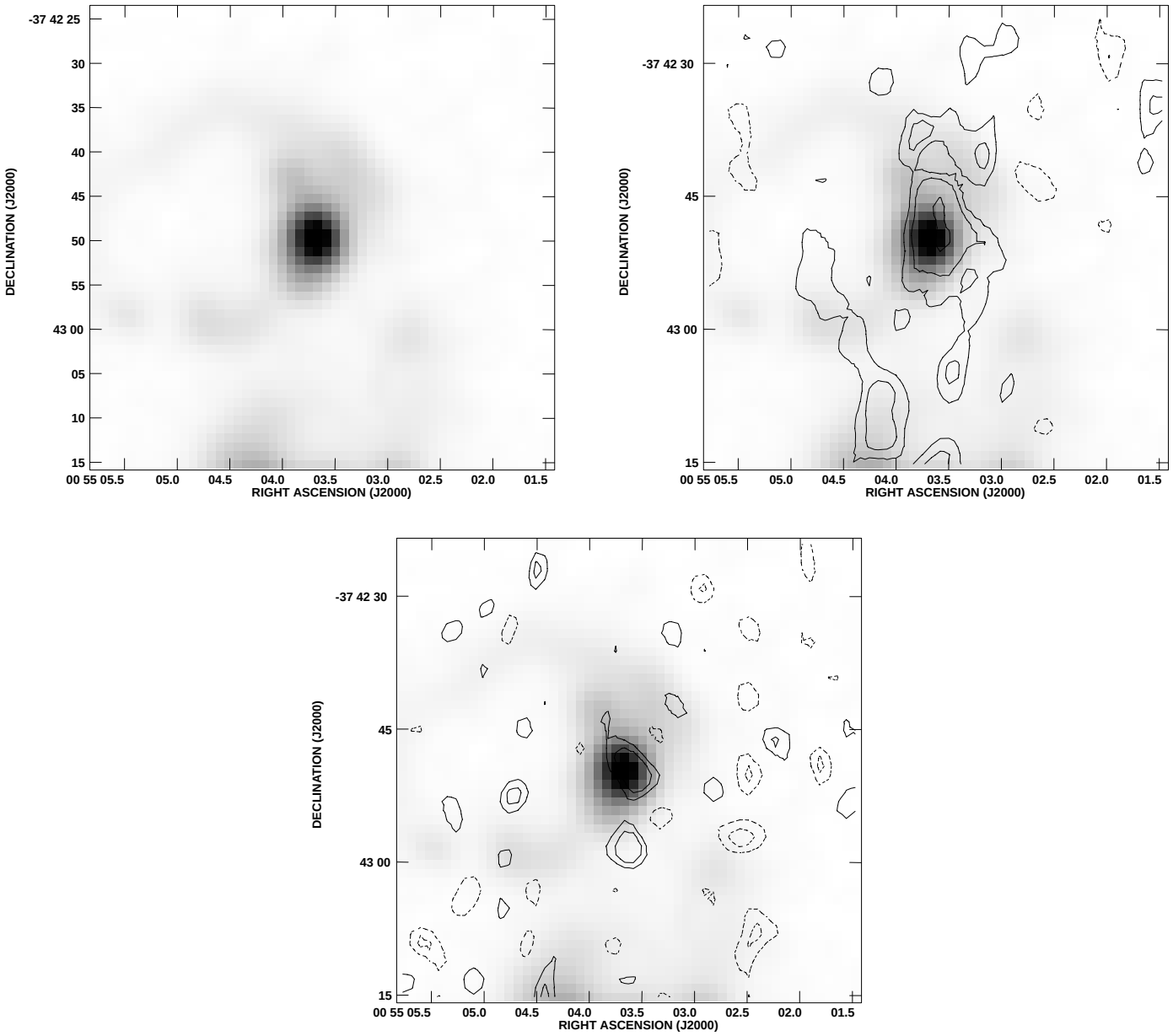

FIG. 15.—Same as Fig. 2, but for the candidate radio SNR R11 in the H II region Deharveng 118A

SNRs that result from low-mass progenitors (Type Ia supernovae), typically found far from star-forming regions. Obvious exceptions are the Balmer dominated SNRs (such as Tycho and SN 1006 in our own Galaxy). However, it is important to note that these Balmer-dominated SNRs are quite young. They have modest diameters and are not at all representative of the SNRs in the NGC 300 sample. In contrast, SNRs that have massive star progenitors (Type II supernovae) are located within or near H II regions and are more likely to be optically confused.

If these selection effects are indeed important then it is possible that the environments of the detected SNRs may differ systematically depending on the manner in which they are selected. The optically selected SNRs, for example, may, on average, lie in regions of lower gas density because they are biased against star-forming regions (which typically tend to have higher than average gas densities). Evidence to this effect can be found in the paper by Magnier et al. (1997). They find that of over 200 optically identified SNRs in M31, only six are detected with the High-Resolution Imager (*HRI*) onboard the *ROSAT* satellite. While much of this lack of overlap can be attributed to poor *HRI* sensitivity, their analysis of the preshock gas densities indicates that the optically identified SNRs are indeed expanding in regions of very low gas density ($n_e < 0.1$ cm^{-3}). In other words, if the optically identified SNRs were expanding in denser media (such as those found in star-forming regions) then they should have been detected by the *HRI*. Thus, the issue is not just sensitivity but also the preselected environment.

The results of Magnier et al. (1997) strengthen our hypothesis that optical confusion leads to a preselection of SNRs expanding into low-density media. A similar argument has been made in comparing the radio and optically selected SNRs in NGC 6946 (Lacey, Duric, & Goss 1997, 2000). Radio and X-ray emission from SNRs seems to be sensitive to preshock gas density. In fact, the Venn diagram

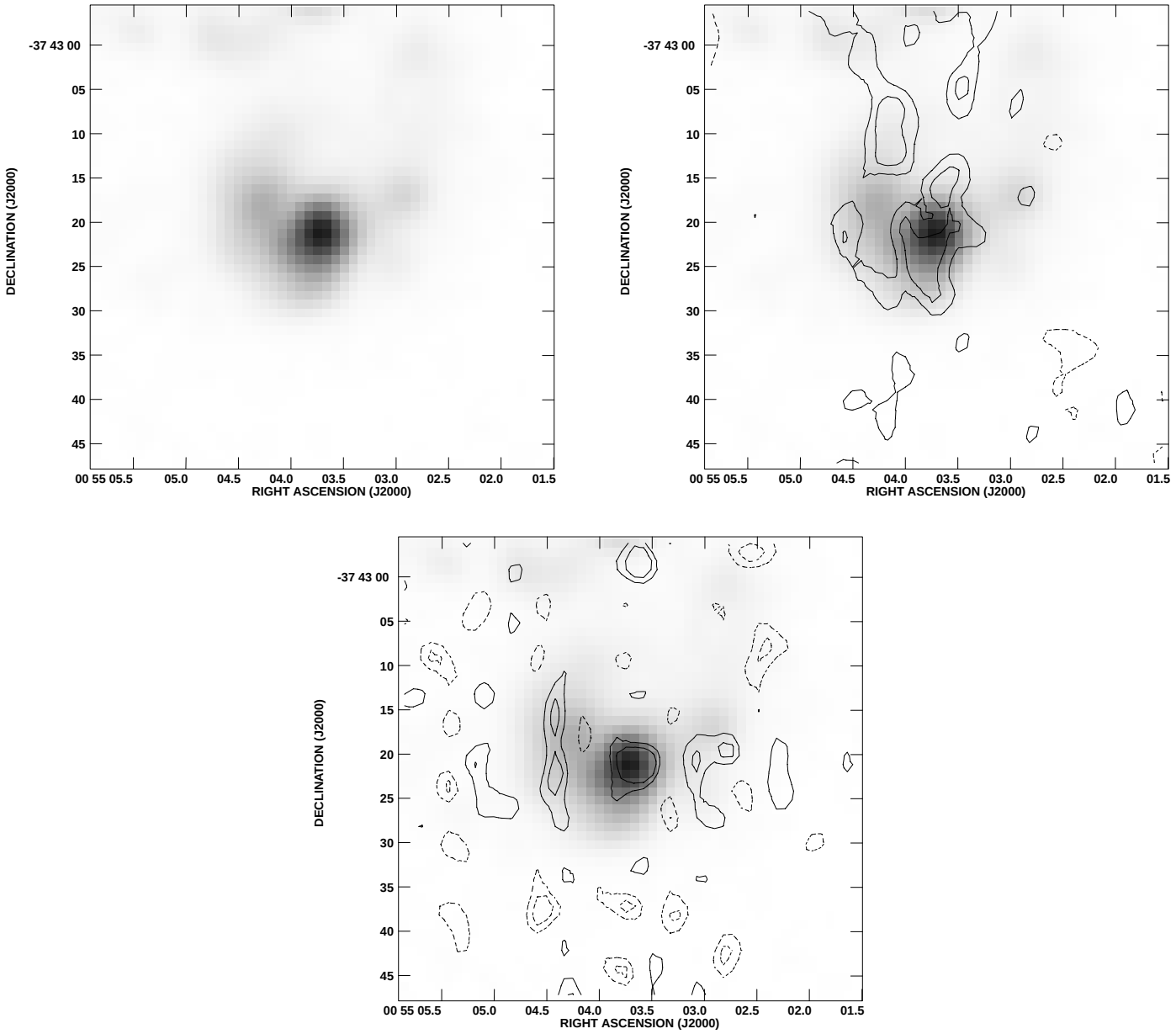

FIG. 16.—Same as Fig. 2, but for the candidate radio SNR R12 in the H II region Deharveng 119A

for NGC 300 shows that two-thirds of the X-ray–selected candidates are also radio-selected SNRs while only one-third are optically identified SNRs. We note that there is NO overlap between the optically selected and X-ray–selected SNRs unless there is also radio emission present. It therefore seems plausible that the optically selected SNRs in NGC 300 have low enough levels of X-ray and radio emission to be largely undetected, while those SNRs selected by X-ray and radio means are undetectable by optical search methods.

We point out that the three optically selected SNRs that possess considerable emission at another wavelength—N300-S10, N300-S11 and N300-S26—all lie in regions of enhanced density, namely the perimeters of H II regions. The perimeter location reduces the amount of optical confusion and permits the source to be detected by optical methods. However, the density at that location is still large enough to facilitate the production of considerable X-ray and radio emission.

7. CONCLUSIONS

1. The nearby spiral galaxy NGC 300 has been studied in the X-ray, optical, and radio wavelengths for the presence of SNRs. This search has made use of combined observations of the galaxy by the PSPC instrument aboard the *ROSAT* satellite, an Hα image of the galaxy, and new VLA 6 and 20 cm observations of the galaxy. We have examined the X-ray and radio properties of the SNRs previously identified in the optical by BL97, and we have complemented this by searching for previously unknown SNRs. We have accomplished this by constructing radio and X-ray–selected samples of SNR candidates.

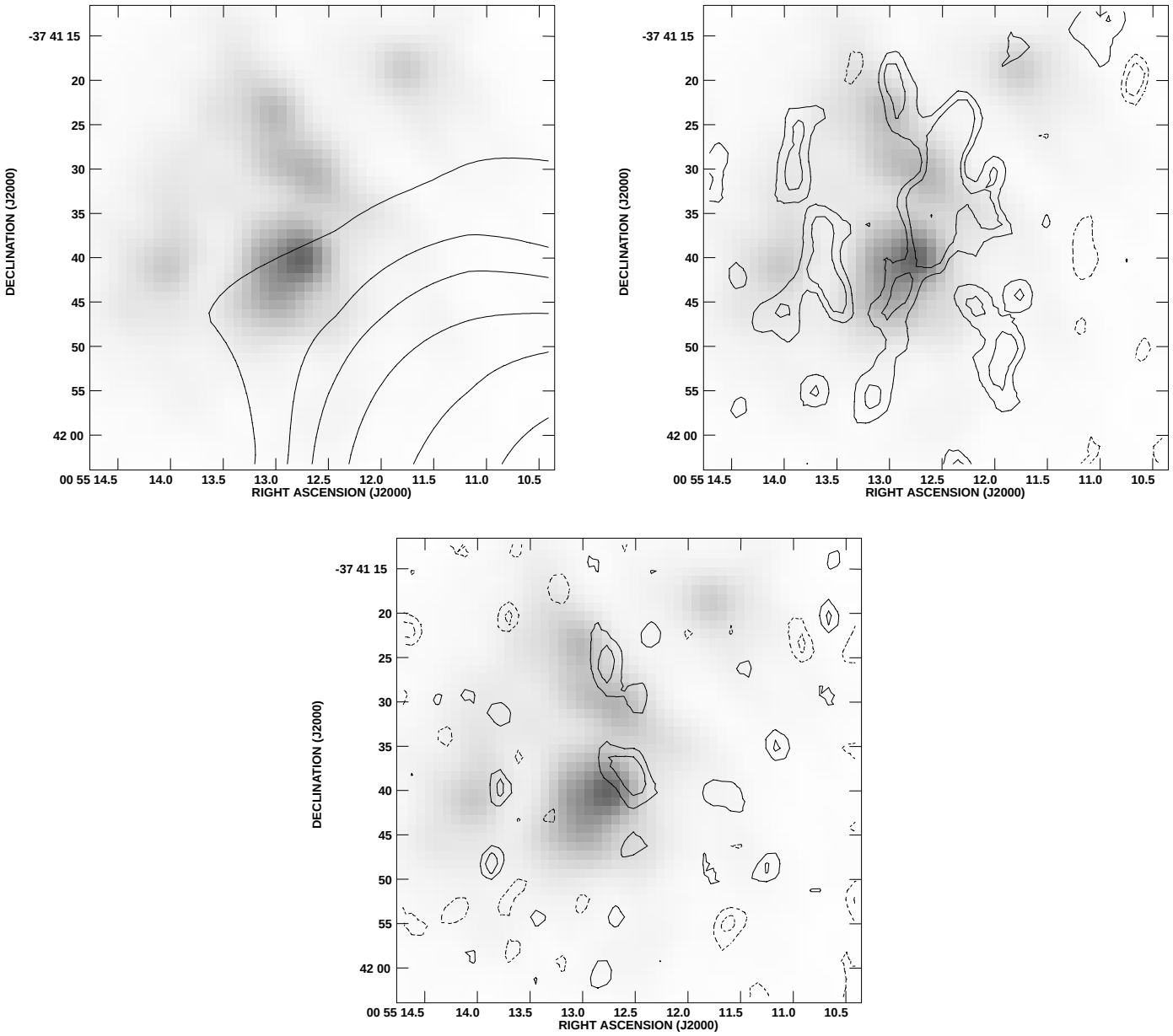

FIG. 17.—Same as Fig. 2, but for the candidate radio SNR R13 in the H II region Deharveng 137A

2. Only two of the optically identified SNRs (N300-S10 and N300-S26) possess both X-ray and nonthermal radio emission. A third, N300-S11, possesses nonthermal radio emission but has no X-ray emission. In general, X-ray and radio emission from optically identified SNRs is not detected, possibly indicating a selection effect inherent in optical searches for SNRs. The detection of X-ray emission from N300-S10 and N300-S26 is significant, given the conclusion by BL97 that these objects are surrounded by a dense interstellar medium, and that X-ray emission should be correlated with density in the vicinity of a SNR. In agreement with the data of Lacey et al. (1997) for the optically identified SNRs in NGC 6946, the optically identified SNRs in NGC 300 tend to be undetected in the radio.

3. A search for nonthermal radio sources at 6 cm and 20 cm (with a minimum detection level of 3 σ) that are close to or within H II regions has yielded 14 new radio-emitting candidate SNRs. Of these 14 sources, two (R2 and R4) possess counterparts at the 3 σ level. Although our VLA survey has also yielded many nonthermal sources *not* associated with regions of Hα emission, there is no practical way to separate these particular sources from background sources. Consequently, our sample of radio-selected SNRs is biased toward those SNRs lying near star-forming regions.

4. An X-ray–selected sample of SNR candidates was constructed by searching for soft-spectrum X-ray sources that are coincident with regions of Hα emission. This search yielded six candidate X-ray SNRs: two (4 and 10) are associated with optically identified SNRs, while two others (2 and 5) are associated with candidate radio SNRs, and the remaining two are new candidate SNRs.

5. Through a campaign spanning three regimes of the electromagnetic spectrum (X-ray, optical, and radio) we have discovered 16 new candidate SNRs. Spectral properties (namely, the counterparts at all three wavelengths) of

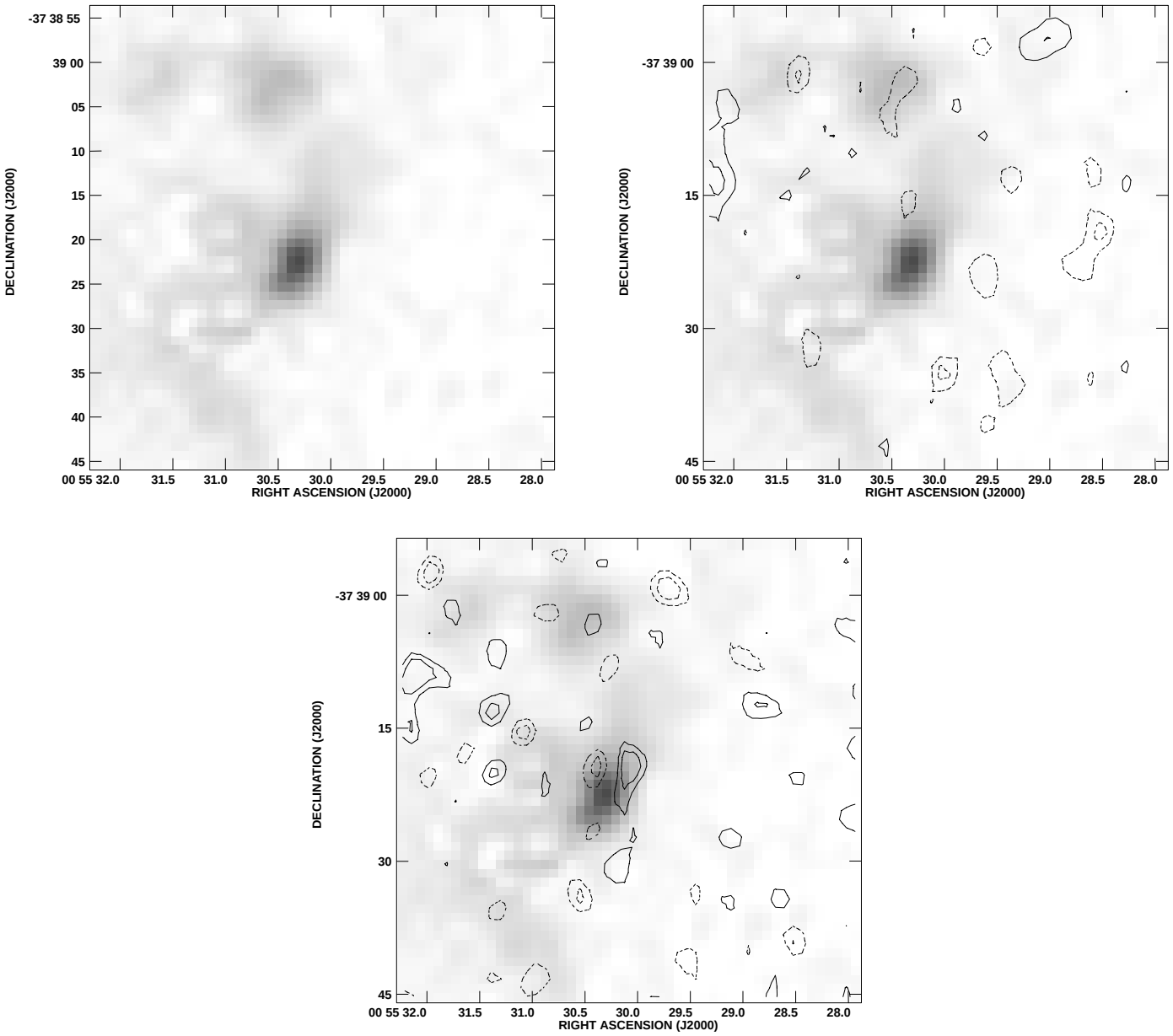

FIG. 18.—Same as Fig. 2, but for the candidate radio SNR R14 in the H II region Deharveng 153

these new sources are listed in Table 10. The considerable number of new candidate SNRs revealed by this survey illustrates the effectiveness of using a multiwavelength campaign like the one presented in this paper. The fact that these new candidates were missed in the optical surveys suggests a possible selection effect. SNRs identified through optical methods may represent only the SNRs located in regions of low density. Those SNRs that are located in dense, star-forming regions are likely to be confused by distributed emission from H II regions. The radio-selected SNRs suffer from the opposite effect: these can only be located if they are associated with H II regions and are therefore biased toward regions of higher density. Figure 19 illustrates the number of SNRs found at each wavelength, as well as the number of SNRs found at multiple wavelengths. The fact that the three sets of candidate SNRs demonstrate little overlap is consistent with these opposing selection effects. The effect is a strong function of distance. Though it is not important in surveys of the Galaxy and the Magellanic Clouds it becomes increasingly important as one moves to M33 and beyond to the Sculptor Group galaxies such as NGC 300. We conclude that a multifrequency search for SNRs is required to uniformly sample the SNR population of a galaxy.

This study has found candidate SNRs with a wide range of spectral properties in a diversity of environments. Further analysis of the SNR environments will help constrain models of the spectral evolution of SNRs. The results of such an analysis will be reported in a future paper. Future work will also include extending this multiwavelength survey to examine other nearby galaxies.

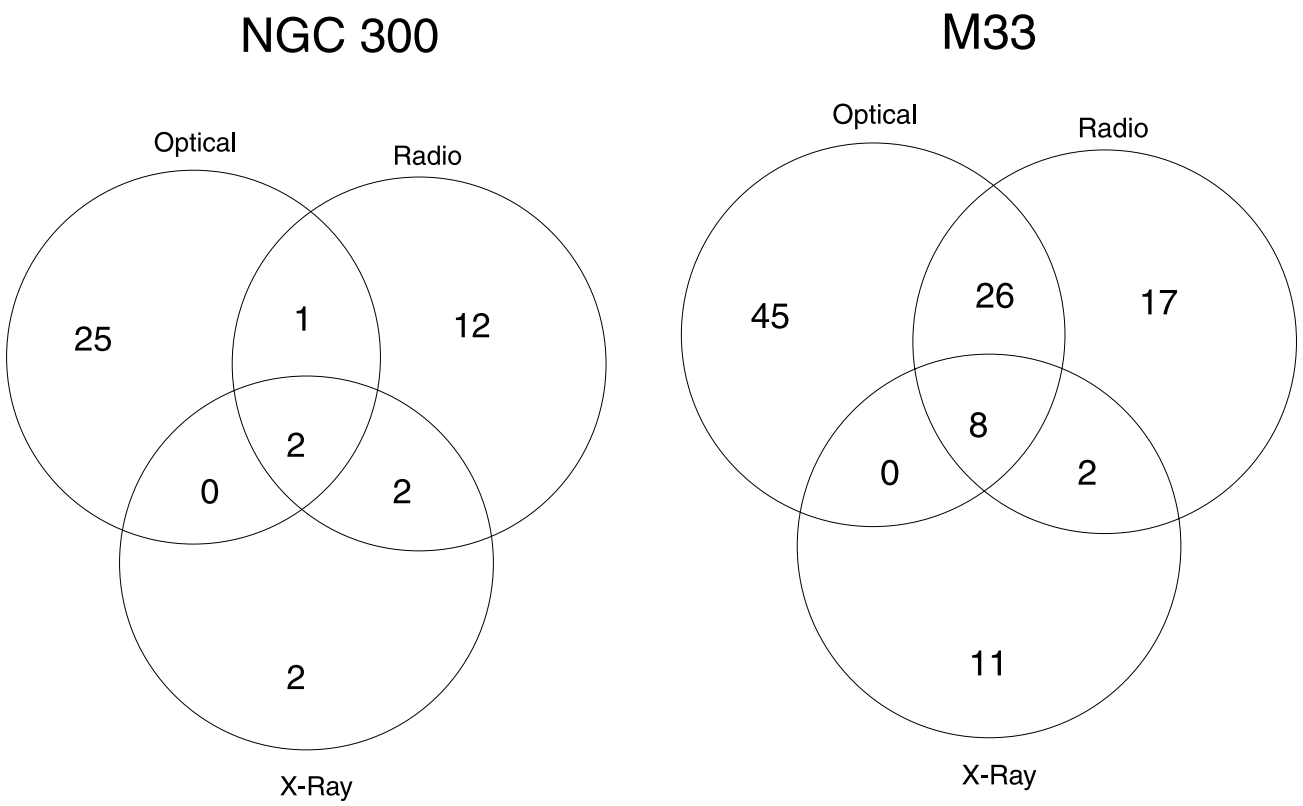

FIG. 19.— Venn diagram illustrating the intersection of all three sets of candidate SNRs in NGC 300 (Fig. 19*a*, *left*) and in M33 (Fig. 19*b*, *right*). Notice the limited intersection between all three groups of SNRs in both galaxies, particularly in NGC 300.

TABLE 9

MEAN RATIO VALUES AND MAXIMUM VALUES FOR ARTIFICAL SNRS

				Convolved Image								
	Unconvolved Image			3″			6″			9″		
SNR	Mean	RMS	Max	Mean	RMS	Max	Mean	RMS	Max	Mean	RMS	Max
I1	0.81	0.19	1.21	0.68	0.07	0.79	0.66	0.06	0.73	0.63	0.06	0.71
I2	0.56	0.13	0.88	0.49	0.08	0.61	0.45	0.04	0.51	0.38	0.03	0.42
I3	0.66	0.14	0.94	0.63	0.10	0.89	0.63	0.05	0.74	0.63	0.03	0.70
I4	0.74	0.15	1.05	0.67	0.09	0.79	0.68	0.05	0.82	0.68	0.07	0.82
P1.....	0.51	0.16	0.87	0.36	0.15	0.59	0.29	0.10	0.45	0.21	0.06	0.33
P2.....	0.29	0.10	0.46	0.25	0.08	0.38	0.22	0.05	0.31	0.18	0.03	0.24
P3.....	0.19	0.04	0.28	0.17	0.02	0.21	0.16	0.01	0.17	0.14	0.01	0.15
P4.....	0.23	0.08	0.50	0.20	0.03	0.27	0.17	0.02	0.21	0.15	0.01	0.17
E1.....	0.13	0.02	0.16	0.13	0.14	0.15	0.13	0.01	0.14	0.12	0.00	0.13
E2.....	0.16	0.04	0.24	0.16	0.02	0.20	0.15	0.01	0.17	0.14	0.01	0.15
E3.....	0.11	0.01	0.14	0.11	0.00	0.12	0.11	0.00	0.11	0.11	0.00	0.11
E4.....	0.14	0.02	0.18	0.14	0.01	0.15	0.14	0.01	0.15	0.14	0.00	0.14

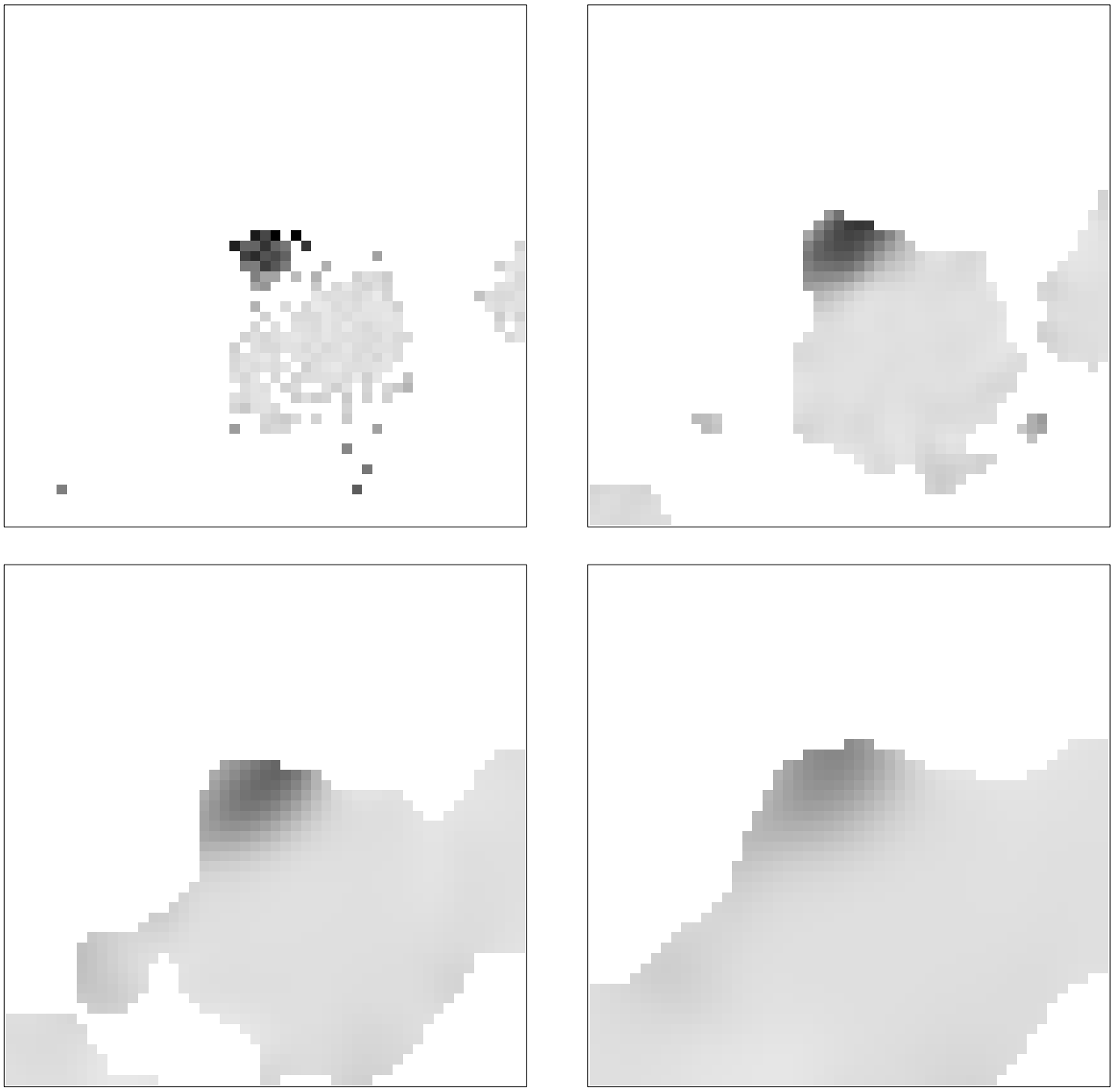

FIG. 20.—[S II]/Hα ratio images of the artificial SNR P1. In the upper right, the ratio map without any convolving is depicted. Upper right, lower left, and lower right show the ratio map for the source after 3″ convolving, 6″ convolving, and 9″ convolving, respectively.

TABLE 10

CROSS-REFERENCES OF ALL NEW CANDIDATE SNRs[a]

SNR	R.A. (J2000.0)	Decl. (J2000.0)	Radio Counterpart?	Optical Counterpart?	X-ray Counterpart?
SNR 1	00 54 31.7	−37 38 16	...	D29	No. 1
SNR 2	00 54 38.2	−37 41 47	R1	D39	...
SNR 3	00 54 38.4	−37 42 42	R2	D40	No. 2
SNR 4	00 54 43.4	−37 43 11	R3	D53A	...
SNR 5	00 54 44.9	−37 41 10	R4	D60	...
SNR 6	00 54 45.1	−37 41 49	R5	Uncataloged H II region	No. 5
SNR 7	00 54 50.3	−37 40 31	R6	D76A	...
SNR 8	00 54 51.1	−37 40 59	R7	D80	...
SNR 9	00 54 51.1	−37 41 45	R8	D81	...
SNR 10.....	00 54 51.3	−37 46 22	R9	D82	...
SNR 11.....	00 54 51.8	−37 39 39	R10	D84	...
SNR 12.....	00 55 03.6	−37 42 49	R11	D118A	...
SNR 13.....	00 55 03.7	−37 43 21	R12	D119A	...
SNR 14.....	00 55 12.6	−37 41 38	R13	D137A	...
SNR 15.....	00 55 20.4	−37 38 34	...	Uncataloged H II region	No. 11
SNR 16.....	00 55 30.1	−37 39 20	R14	D153	...

NOTE.—Units of right ascension are hours, minutes, and seconds, and units of declination are degrees, arcminutes, and arcseconds.

[a] In this table, the radio counterparts are the radio sources presented in Table 3, the optical counterparts are the H II regions cataloged by D88, and the X-ray counterparts are the X-ray sources listed in Table 4.

We thank the anonymous referee for many constructive comments and suggestions that have improved this paper. T. G. P. acknowledges useful discussions with William Blair and Shawn Gordon, as well as assistance by a Research, Project and Travel Grant awarded by the Office of Graduate Studies at the University of New Mexico. This research has made use of the NASA/IPAC Extragalactic Database (NED) which is operated by the Jet Propulsion Laboratory, Caltech, under contract with the National Aeronautics and Space Administration.[4] The *ROSAT* project is supported by the German Bundesministerium für Bildung und Forschung (BMBF) and the Max-Planck-Gesellschaft (MPG).

[4] The NASA/IPAC Extragalactic Database (NED) is operated by the Jet Propulsion Laboratory, California Institute of Technology, under contract with the National Aeronautics and Space Administration. N.E.D., IPAC 100-22, Caltech, Pasadena, CA 91125.

REFERENCES

Blair, W. P., Kirshner, R. P., & Chevalier, R. A. 1981, ApJ, 247, 879
Blair, W. P., & Long, K. S. 1997, ApJS, 108, 261 (BL97)
Braun, R., & Walterbos, R. A. M. 1993, A&AS, 98, 327
Deharveng, L., Caplan, J., Lequeux, J., Azzopardi, M., Breysacher, J., Tarenghi, M., & Westerlund, B. 1988, A&AS, 73, 407 (D88)
D'Odorico, S., Dopita, M. A., & Benvenuti, P. 1980, A&AS, 40, 67 (DDB80)
Duric, N., Gordon, S. M., Goss, W. M., Viallefond, F., & Lacey, C. 1995, ApJ, 445, 173
Ferguson, A. M. N., Wyse, R. F. G., Gallagher, J. S., III, & Hunter, D. A. 1996, AJ, 111, 2265
Freedman, W. L., Madore, B. F., Hawley, S. L., Horowitz, I. K., Mould, J., & Sallmen, S. 1992, ApJ, 396, 80
Freedman, W. L., Wilson, C. D., & Madore, B. F. 1991, ApJ, 372, 455
Gordon, S. M., Duric, N., Kirshner, R. P., Goss, W. M., & Viallefond, F. 1999, ApJS, 120, 247
Gordon, S. M., Kirshner, R. P., Duric, N., & Long, K. S. 1993, ApJ, 418, 743
Gordon, S. M., Kirschner, R. P., Long, K. S., Blair, W. P., Duric, N., & Smith, R. C. 1998, ApJS, 117, 89
Hoopes, C. G., Walterbos, R. A. M., & Greenawalt, B. E. 1996, AJ, 112, 1429
Itoh, H., & Masai, K. 1989, MNRAS, 236, 885
Lacey, C. K., Duric, N., & Goss, W. M. 1997, ApJS, 109, 417
———. 2000, ApJ, submitted
Long, K. S., Blair, W. P., Kirshner, R. P., & Walker, P. F. 1990, ApJS, 72, 61
Long, K. S., Charles, P. A., Blair, W. P., & Gordon, S. M. 1996, ApJ, 466, 750
Lozinskaya, T. A., Silchenko, O. K., Helfand, D. J., & Goss, W. M. 1998, AJ, 116, 2328
Magnier, E. A., Primini, F. A., Prins, S., van Paradijs, J., & Lewin, W. H. G. 1997, ApJ, 490, 649
Magnier, E. A., Prins, S., van Paradijs, J., Lewin, W. H. G., Supper, R., Hasinger, G. Pietsch, W., & Trümper, J. 1995, A&AS, 114, 215
Mathewson, D. S., & Clarke, J. N. 1972, ApJ, 178, L105
———. 1973a, ApJ, 180, 725
———. 1973b, ApJ, 182, 697
Matonick, D. M., & Fesen, R. A. 1997, ApJS, 112, 49
Matonick, D. M., Fesen, R. A., Blair, W. P., & Long, K. S. 1997, ApJS, 113, 333
Mitchell, K. J., & Condon, J. J. 1985, AJ, 90, 1957
Puche, D., & Carignan, C. 1988, AJ, 95, 1025
Puche, D., Carignan, C., & Bosma, A. 1990, AJ, 100, 1468
Read, A. M., Ponman, T. J., & Strickland, D. K. 1997, MNRAS, 286, 626 (RPS97)
Reed, J. E., Hester, J. J., Fabian, A. C., & Winkler, P. F. 1995, ApJ, 440, 706
Smith, R. C. 1997, AJ, 114, 2664
Smith, R. C., Kirshner, R. P., Blair, W. P., Long, K. S., & Winkler, P. F. 1993, ApJ, 407, 564
Trümper, J. 1992, QJRAS, 33, 165
Tully, R. 1988, Nearby Galaxies Catalog (Cambridge: Cambridge Univ. Press)
Zang, Z., Warwick, R. S., & Meurs, E. J. A. 1997, Irish Astron. J., 24, 45